Heat transfer and entropy generation in a parabolic trough receiver with wall-detached twisted tape inserts

CrossMark

Aggrey Mwesigye [a], Tunde Bello-Ochende [b, *], Josua P. Meyer [c]

[a] Department of Mechanical Engineering, Mechatronics and Industrial Design, Tshwane University of Technology, Private Bag X680, Pretoria 0001, South Africa
[b] Department of Mechanical Engineering, University of Cape Town, Private Bag X3, Rondebosch 7701, South Africa
[c] Department of Mechanical and Aeronautical Engineering, University of Pretoria, Private Bag X20, Hatfield 0028, South Africa

A B S T R A C T

In this paper, heat transfer enhancement in a parabolic trough receiver using wall-detached twisted tape inserts was numerically investigated. The resulting heat transfer, fluid friction and thermodynamic performance were determined and presented. The flow was considered fully developed turbulent, with Reynolds numbers in range $10\ 260 \leq Re_p \leq 1\ 353\ 000$ depending on the fluid temperature. The twisted tape's twist ratio and width ratio vary in the range 0.50–2.00 and 0.53–0.91, respectively. The numerical investigations are based on a finite volume method, with the realisable $k-\varepsilon$ model for turbulence closure. The study shows considerable increase in heat transfer performance of about 169%, reduction in absorber tube's circumferential temperature difference up to 68% and increase in thermal efficiency up to 10% over a receiver with a plain absorber tube. An entropy generation analysis shows the existence of a Reynolds number for which there is minimum entropy generation for each twist ratio and width ratio. The optimal Reynolds number increases with increasing twist ratio and reducing width ratios. The maximum reduction in the entropy generation rate was about 58%. Correlations for heat transfer and fluid friction performance for the range of parameters considered were also derived and presented.

© 2015 Elsevier Masson SAS. All rights reserved.

1. Introduction

Parabolic trough systems represent the most commercially and technically developed technology for concentrated solar power [1–3]. Several research initiatives are still under way to further improve their performance and reduce the cost of energy from these systems [1,3,4]. With the availability of lightweight materials, increasing concentrator sizes and concentration ratios is one way of improving performance and reducing costs [5,6].

With higher concentration ratios, the increased heat fluxes and possible increase of the absorber tube's circumferential temperature difference will necessitate improved heat transfer. Heat transfer enhancement is one way of achieving improved heat transfer performance in heat exchangers and is widely used for several industrial applications. As such, several heat transfer enhancement techniques have been developed and investigated,

detailed reviews of such techniques are detailed by Bergles [7], Manglik [8] and Webb [9]. Heat transfer enhancement in heat exchangers and other thermal applications has several benefits such as heat exchanger weight and size reduction, reduction in device temperatures and reduction in the temperature difference between process fluids.

In parabolic trough receivers, the non-uniformity of the absorber tube's circumferential temperature leads to thermal stresses and can cause breakage of the receiver's glass cover in cases of high absorber tube circumferential temperature differences [1,10]. Further still, several studies on thermal performance of receivers have shown that the higher the absorber tube temperature, the higher the receiver thermal losses [11–13]. Moreover, as parabolic trough systems with high optical efficiencies and high concentration ratios become feasible [5], high heat fluxes and high absorber tube's circumferential temperature difference will result. As such, improved heat transfer performance will be essential to minimise absorber tube temperature gradients as well as improve the performance and reliability of the receiver.

For these reasons, heat transfer enhancement in parabolic trough receivers is receiving considerable attention. Passive heat

* Corresponding author. Tel.: +27 21 650 3673; fax: +27 21 650 3240.
E-mail addresses: tunde.bello-ochende@uct.ac.za (T. Bello-Ochende), josua.meyer@up.ac.za (J.P. Meyer).

Nomenclature

A	area, m^2
A_c	collector's projected aperture area, m^2
A_r	absorber tube's projected area, m^2
Be	Bejan number
C_1, C_2, C_μ	turbulent model constants
c_f	skin friction coefficient
c_p	specific heat capacity, $J\ kg^{-1}\ K^{-1}$
C_R	concentration ratio
DNI	direct normal irradiance, $W\ m^{-2}$
d_{gi}	glass cover inner diameter, m
d_{go}	glass cover outer diameter, m
d_{ri}	absorber tube inner diameter, m
d_{ro}	absorber tube outer diameter, m
f	Darcy friction factor
G	mass flux, $kg\ m^{-2}\ s^{-1}$
G_k	generation of turbulence kinetic energy due to mean velocity gradients, $kg\ m^{-1}\ s^{-3}$
h	heat transfer coefficient, $W\ m^{-2}\ K^{-1}$
h_w	wind convection heat transfer coefficient, $W\ m^{-2}\ K^{-1}$
H	twisted tape half pitch, m
I_b	direct solar radiation, $W\ m^{-2}$
k	turbulent kinetic energy, $m^2\ s^{-2}$
L	length, m
$\dot{m}$	mass flow rate, $kg\ s^{-1}$
Nu	Nusselt number
$N_{s,en}$	enhancement entropy generation ratio $= (S_{gen})_{en}/(S_{gen})_p$
P	pressure, Pa
Pr	Prandtl number
q'	heat transfer rate per meter length, $W\ m^{-1}$
q''	heat flux, $W\ m^{-2}$
Re	Reynolds number
S	modulus of the mean rate-of-strain tensor, s^{-1}
S_{ij}	rate of linear deformation tensor, s^{-1}
S_{gen}	entropy generation rate due to heat transfer and fluid friction, $W\ K^{-1}$
S'_{gen}	entropy generation due to heat transfer and fluid friction per unit length, $W\ m^{-1}\ K^{-1}$
$(S_{gen})_H$	entropy generation due to heat transfer, $W\ K^{-1}$
$(S_{gen})_F$	entropy generation due to fluid friction, $W\ K^{-1}$
$(S'_{gen})_H$	entropy generation due to heat transfer per unit length, $W\ m^{-1}\ K^{-1}$
$(S'_{gen})_F$	entropy generation due to fluid friction per unit length, $W\ m^{-1}\ K^{-1}$
S'''_{gen}	volumetric entropy generation, $W\ m^{-3}\ K^{-1}$
$(S'''_{gen})_F$	volumetric entropy generation due to fluid friction, $W\ m^{-3}\ K^{-1}$
$(S'''_{gen})_H$	volumetric entropy generation due to heat transfer, $W\ m^{-3}\ K^{-1}$
$S'''_{PROD,VD}$	entropy production by direct dissipation, $W\ m^{-3}\ K^{-1}$
$S'''_{PROD,TD}$	entropy production by turbulent dissipation, $W\ m^{-3}\ K^{-1}$
$S'''_{PROD,T}$	entropy production by heat transfer with mean temperatures, $W\ m^{-3}\ K^{-1}$
$S'''_{PROD,TG}$	entropy production by heat transfer with fluctuating temperatures, $W\ m^{-3}\ K^{-1}$
T	temperature, K
u_m	mean velocity, $m\ s^{-1}$
V	volume, m^3
V_w	wind speed, $m\ s^{-1}$
u_i, u_j	averaged velocity components, $m\ s^{-1}$
u', v', w'	fluctuations from mean velocity, $m\ s^{-1}$
u_τ	friction velocity, $m\ s^{-1}$
$\dot{V}$	volumetric flow rate, $m^3\ s^{-1}$
W	twisted tape width, m
W_a	collector aperture width, m
$\dot{W}_p$	pumping power, W
$\tilde{w}$	twisted tape width ratio
x_i, x_j	spatial coordinates, m
x, y, z	Cartesian coordinates
y^+	dimensionless wall coordinate
$\tilde{y}$	twisted tape width ratio
$-\rho\overline{u'_i u'_j}$	Reynolds stresses, $N\ m^{-2}$
ΔP	pressure drop, Pa

Greek letters

α	thermal diffusivity, $m^2\ s^{-1}$
α_t	turbulent thermal diffusivity, $m^2\ s^{-1}$
δ_{ij}	Kronecker delta
ε	turbulent dissipation rate, $m^2\ s^{-3}$
λ	fluid thermal conductivity, $W\ m^{-1}\ K^{-1}$
η	turbulence model parameter $= Sk/\varepsilon$
η_{th}	thermal efficiency, %
η_{el}	power block electrical efficiency, %
φ_r	rim angle
ϕ	absorber tube's circumferential temperature difference, K
ρ	density, $kg\ m^{-3}$
α_t	turbulent thermal diffusivity, $m^2\ s^{-1}$
σ_ε	turbulent Prandtl number for ε
$\sigma_{h,t}$	turbulent Prandtl number for energy
σ_k	turbulent Prandtl number for k
τ_g	glass cover transmissivity
τ_w	wall shear stress
θ	receiver circumferential angle
μ	viscosity, Pa s
μ_t	turbulent viscosity, Pa s
μ_τ	friction velocity, $m\ s^{-1}$
μ_{eff}	effective viscosity, Pa s
ν	kinematic viscosity, $m^2\ s^{-1}$
χ	thermal enhancement factor

Subscripts

amb	ambient state
$bulk$	bulk fluid state
en	enhanced absorber tube
$inlet$	absorber tube inlet
$outlet$	absorber tube outlet
i, j, k	general spatial indices
p	plain absorber tube
r, max	absorber tube maximum temperature
r, min	absorber tube minimum temperature
ri	absorber tube inner wall
ro	absorber tube outer wall
sky	sky

Superscripts

$-$	mean value
$\sim$	dimensionless value

transfer enhancement techniques are an attractive method of heat transfer enhancement since no direct power input is required [9]. Several researchers have applied some of the passive heat transfer enhancement techniques to improve the performance of parabolic trough receivers [10,14–16]. Muñoz and Abánades [10] analysed an internally helically finned absorber tube to improving the thermal performance and minimise the circumferential temperature differences in the absorber tube. For the considered flow rates and finned tube designs, the absorber tube temperature difference was reduced by between 15.3 and 40.9%.

Twisted tape inserts have been widely used in many applications given the ease with which they can be made and installed in heat exchangers as well as significant heat transfer enhancement that can be achieved with moderate friction factors [17,18]. The wide application and interest in using twisted tape for both laminar and turbulent flows can be seen in the number of studies dedicated to heat transfer enhancement using twisted tape inserts provided in reviews by Manglik [18], Bergles [7], Webb [9] and many others. Several modifications of the twisted tape inserts have also been widely investigated. These include regularly spaced twisted tape inserts, short length twisted tape inserts, center wing and alternate axes twisted tapes, twisted tapes with cuts, twisted tapes with wire nails, twisted tapes placed separately from the wall and many other modifications. A review on the use of twisted tape inserts for the turbulent flow regime and the different modifications investigated by several researchers was presented by Hasanpour [19]. In this review, favorable enhancement ratios based on constant pressure comparison are reported with the use of twisted tapes in the turbulent flow regime. In another review, Liu and Sakr [20] present a comprehensive review of heat transfer enhancement in passive heat exchangers. In their review, studies on twisted tape inserts with twist ratios in the range 2–12 for both laminar and turbulent flow applications are presented. Nithiyesh and Murugesan [21] also present a review on the use of twisted tape inserts for heat transfer enhancement, twisted tape inserts with twist ratios as low as 1.5 are presented.

The use of twisted tape inserts for solar thermal applications has been investigated by some authors. Jaisankar et al. [22–24] present the results of studies on heat transfer enhancement in solar water-heating systems, using twisted tape inserts. They report an increased heat transfer performance due to the use of twisted tape inserts. Jaisankar et al. [25] experimentally investigated the use of twisted tape inserts with a rod or spacer at the trailing edge in a thermosyphon solar water-heating system. They showed that using rods and spacers at the trailing edge reduced the heat transfer performance by 17–29% respectively, and reduced the pressure drop by 39–47%. In some studies, the combined use of twisted tape inserts with nanofluids has been investigated [26,27]. Enhanced convective heat transfer coefficients and thermal performance were obtained with combined use of twisted tape insert and nanofluid in the laminar and turbulent flow regime, respectively.

To avoid any hot spots and possible degradation of the heat transfer fluid [28], tube inserts are an attractive heat transfer enhancement option for parabolic trough receivers. Therefore, wall detached twisted tape inserts offer a promising alternative compared to other modifications of twisted tape inserts. The use of twisted tape inserts placed separately from tube walls has been investigated in previous studies. Ayub and Al-Fahed [29] first reported an experimental investigation on fluid friction for twisted tape inserts placed separately from the wall. Al-Fahed and Chakroun [30] later investigated the use of wall-separated twisted tape inserts on heat transfer for fully developed turbulent flow. Eiamsa-ard et al. [31] also considered the use of loose-fit twisted tape inserts on heat transfer enhancement in a tube. They report high heat transfer enhancement at the lowest twist ratio and the smallest

clearance ratio. Friction factors were shown to reduce as clearance ratios increased. Zhang et al. [32] presented results of a numerical simulation for multi-longitudinal vortices in a tube induced by triple and quadruple twisted tapes inserts. In both cases, the twisted tape inserts are placed separately from the tube wall. The Nusselt numbers increased by 171% and 182% for triple and quadruple twisted tapes while the corresponding increase in friction factors was 4.06–7.02 times, respectively. Bas and Ozceyhan [33] presented an experimental investigation on the use of twisted tape inserts placed separately from the wall. Twist ratios of 2.0, 2.5, 3.0, 3.5 and 4.0, clearance ratios of 0.0178 and 0.0357 and Reynolds numbers in the range 5132 and 24 989 were used. The highest heat transfer enhancement was shown to exist at the lowest twist ratio and largest clearance ratio.

Most studies reported in literature use the first law of thermodynamics to characterise the performance of various heat transfer enhancement techniques. For thermal systems, efficient use of energy is crucial to their performance. Therefore, an assessment of the quantity as well as the quality the available energy becomes crucial. The determination of the quality of energy is only possible with the use of the second law of thermodynamics. In the second law of thermodynamics, determination of the entropy generation rates as well the irreversibilities present in the systems and system components is possible. Using the Gouy–Stodola theorem, the entropy generation rates are related to the destruction of available energy [34].

The entropy generation analysis and its minimisation have been widely used for thermodynamic optimisation of thermal systems and components since its introduction by Bejan [35]. However, its application in assessment of heat transfer enhancement techniques is not widespread, but is recommended [34]. Possible reduction of entropy generation rates by minimising heat transfer irreversibilities at high concentration ratios is another benefit of heat transfer enhancement in parabolic trough receivers that is worth investigating.

From the above literature review, several configurations of twisted tape inserts for heat transfer enhancement have been investigated. However, the potential heat transfer enhancement with low twist ratio-wall detached twisted tape inserts has not been investigated. Furthermore, no study has been reported on heat transfer enhancement in parabolic trough receivers with wall detached twisted tape inserts. The use of low twist ratio twisted tapes in parabolic trough receivers has potential to provide high fluid agitation and mixing and a longer helical path, which will lead to high heat transfer rates and reduction in absorber tube's circumferential temperature difference. Moreover, it has been shown in most studies that low twist ratios give higher heat transfer rates, but with high pressure drop penalties [19]. The careful matching of twist ratios and width ratios can result in high heat transfer rates and moderate pressure drop. Therefore, the main objective of this study is to investigate the thermal performance of a parabolic trough receiver with low twist ratio-wall detached twisted tape inserts and to use the entropy generation analysis to determine the resulting irreversibilities as well as optimal configurations and conditions for minimum entropy generation.

2. Physical model

Fig. 1 shows the physical model of a parabolic trough receiver with a twisted tape insert placed separately from the wall. For conventional receivers, the annulus space between the absorber tube and glass cover is evacuated to very low pressures such that only radiation heat transfer takes place. The flow inside the absorber tube becomes periodically fully developed far from the
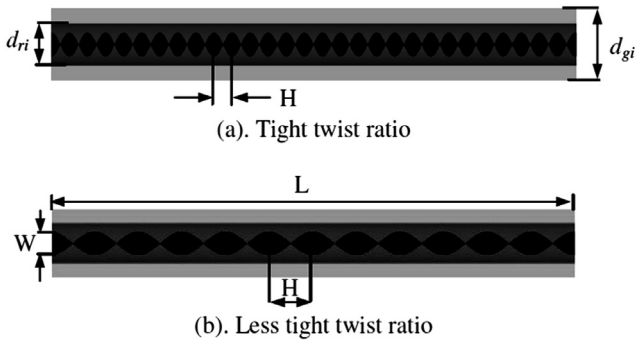
Fig. 1. Physical model of a parabolic trough receiver with wall detached twisted tape inserts.

Table 1
Simulation parameters.

Parameter	Value
(a) General simulation parameters	
Absorber tube inner diameter (cm)	6.6
Absorber tube thickness (cm)	0.2
Glass cover transmissivity, τ_g	0.95
I_b, W m^{-2}	1000
Concentration ratio, C_R	86
Rim angle (degrees)	80
τ_g	0.97
α_r	0.96
ρ	0.96
Twist ratios	0.5–2.0
Width ratios	0.53–0.91
Twisted tape thickness (m)	0.001
Reynolds numbers	$1.03 \times 10^4 – 1.36 \times 10^6$
Inlet temperatures (K)	400 K, 500 K and 600 K

entrance. Therefore, only a periodic module of the receiver is considered. For the absorber tube with a twisted tape insert, the periodic module considered in this study is shown in Fig. 2. Receiver dimensions are taken to be the same as those of commercially available receivers [36]. The absorber tube has an inner diameter (d_{ri}) of 6.6 cm, outer diameter (d_{ro}) of 7.0 cm while the receiver's glass cover has an inner diameter (d_{gi}) of 11.5 cm. The other simulation parameters used in this study are shown in Table 1.

From the physical and computational model, the non-dimensional parameters of the twisted tape used in this study are:

Twist ratio defined as the ratio of the pitch through the 180° turn (H) and the diameter of the absorber tube given by:

$$\tilde{y} = H/d_{ri} \tag{1}$$

The dimensionless twisted tape's width ratio, $\tilde{w}$ defines the clearance between the twisted tape and the absorber tube wall. For zero clearance between the tube and the twisted tape, $\tilde{w} = 1$. The width ratio is given by:

$$\tilde{w} = W/d_{ri} \tag{2}$$
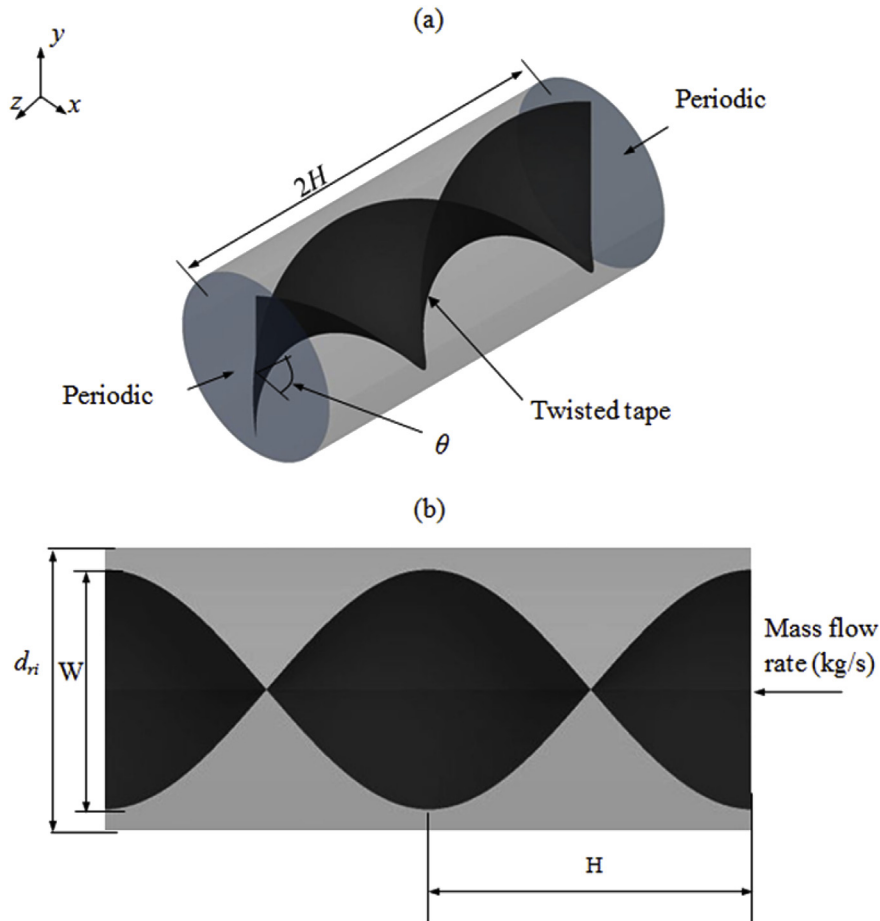
Fig. 2. Computational domain of the receiver's absorber tube: (a) Lateral view, (b) Side view.

The twisted tape could be attached to the tube wall using Teflon attachments manufactured according to twisted tape thickness and width to keep them separated from the tube wall as was done in a study by Bas and Ozceyhan [33] or using some other appropriate mechanism. With low twist ratios, the heat transfer performance is expected to increase, but the fluid friction will also increase. Thus, a combination of lower twist ratios and smaller width ratios could give reasonably high heat transfer rates and moderate pressure drops. Moreover, lower twist ratios provide better fluid agitation and mixing needed in the receiver's absorber tube given the non-uniform heat flux incident on it. Thus, for this study, performance of a parabolic trough receiver with twisted tape inserts having twist ratios in the range 0.5–2.0 and width ratios in the range 0.53–0.93 is investigated.

3. Numerical analysis

3.1. Governing equations

For high heat fluxes and concentration ratios, the expected circumferential temperature differences in the receiver's absorber tube require the use of high flow rates for better heat transfer. Therefore, in this paper, we considered the flow inside the absorber tube to be steady-state and fully developed turbulent. As such, the governing equations are the Reynolds Averaged Navier–Stokes equations and the averaged energy equation [37] given as:

Continuity equation

$$\frac{\partial(\rho u_i)}{\partial x_i} = 0 \tag{3}$$

Momentum equation

$$\frac{\partial}{\partial x_j}(\rho u_i u_j) = -\frac{\partial P}{\partial x_i} + \frac{\partial}{\partial x_j}\left[\mu\left(\frac{\partial u_i}{\partial x_j} + \frac{\partial u_j}{\partial x_i}\right) - \frac{2}{3}\mu\frac{\partial u_i}{\partial x_i}\delta_{ij} - \rho\overline{u_i' u_j'}\right] \tag{4}$$

Energy equation

$$\frac{\partial}{\partial x_j}(\rho u_j c_p T) = \frac{\partial}{\partial x_j}\left(\lambda\frac{\partial T}{\partial x_j} + \frac{\mu_t}{\sigma_{h,t}}\frac{\partial(c_p T)}{\partial x_j}\right) + u_j\frac{\partial P}{\partial x_j}$$
$$+ \left[\mu\left(\frac{\partial u_i}{\partial x_j} + \frac{\partial u_j}{\partial x_i}\right) - \frac{2}{3}\mu\frac{\partial u_i}{\partial x_i}\delta_{ij} - \rho\overline{u_i' u_j'}\right]\frac{\partial u_i}{\partial x_j} \tag{5}$$

where $-\rho\overline{u_i' u_j'}$ are the Reynolds stresses, u_i, u_j are the time-averaged velocity components in the i- and j-directions respectively, T is the time-averaged temperature, P is the time averaged pressure and λ is the fluid thermal conductivity. The Reynolds stresses are related to the mean velocity gradients using the Boussinesq approach through [37].

$$-\rho\overline{u_i' u_j'} = \mu_t\left(\frac{\partial u_i}{\partial x_j} + \frac{\partial u_j}{\partial x_i}\right) - \frac{2}{3}\left(\rho k + \mu_t\frac{\partial u_k}{\partial x_k}\right)\delta_{ij} \tag{6}$$

Where k is the turbulent kinetic energy per unit mass given by

$$k = \frac{1}{2}\left(\overline{u'^2} + \overline{v'^2} + \overline{w'^2}\right) \tag{7}$$

This approach reduces the computational cost compared to solving the transport equations for each term in the Reynolds stress tensor. A number of turbulence models based on the Boussinesq approach have been developed to solve the closure problem in Eqs. (3)–(5). The k–ε models are the most widely used and validated models for most flows present in engineering applications [37–39]. For this study the realisable k–ε model which is an improvement of the standard k–ε was adopted [37,39]. In the realisable k–ε model, two additional equations are solved for the transport of turbulent kinetic energy and turbulent dissipation rates. These are given as [37].

Turbulent kinetic energy, k

$$\frac{\partial}{\partial x_j}(\rho k u_j) = \frac{\partial}{\partial x_j}\left[\left(\mu + \frac{\mu_t}{\sigma_k}\right)\frac{\partial k}{\partial x_j}\right] + G_k - \rho\varepsilon \tag{8}$$

Turbulent dissipation, ε

$$\frac{\partial}{\partial x_j}(\rho\varepsilon u_j) = \frac{\partial}{\partial x_j}\left[\left(\mu + \frac{\mu_t}{\sigma_\varepsilon}\right)\frac{\partial\varepsilon}{\partial x_j}\right] + \rho C_1 S\varepsilon - \rho C_2\frac{\varepsilon^2}{k + \sqrt{\nu\varepsilon}} \tag{9}$$

Where

G_k represents production of turbulent kinetic energy and is modeled the same way for all the k–ε models as

$$G_k = -\rho\overline{u_i' u_j'}\frac{\partial u_j}{\partial x_i} \tag{10}$$

Combining Eq. (6) with Eq. (10) gives

$$G_k = \mu_t S^2 \tag{11}$$

The eddy viscosity is given by

$$\mu_t = \rho C_\mu\frac{k^2}{\varepsilon} \tag{12}$$

In the realisable k–ε, C_μ is not constant and is determined from empirical relations. The detailed determination of C_μ is given in Ref. [37]. The model constants for the k–ε realisable model are:

$$C_1 = \max\left[0.43, \frac{\eta}{\eta + 5}\right], \quad \eta = S\frac{k}{\varepsilon}, \quad S \equiv \sqrt{2S_{ij}S_{ij}}, \quad C_2 = 1.9,$$
$$\sigma_k = 1, \quad \sigma_\varepsilon = 1.2,$$

S_{ij} represents the rate of linear deformation of a fluid element. In total, there are nine components in three dimensions, of which three are linear elongation deformation components and six are shearing and deformation components [38].

$$S_{ij} = \frac{1}{2}\left(\frac{\partial u_i}{\partial x_j} + \frac{\partial u_j}{\partial x_i}\right) \tag{13}$$

3.2. Entropy generation

The entropy generation method is widely used for the design and optimisation of thermal systems and system components. This method has proved an important design tool and has been used by several researchers for thermodynamic optimisation [40–44]. It entails determining the irreversibilities occurring in systems and system components and determining configurations for which these irreversibilities are minimum. Minimum entropy generation corresponds to the maximum power output, since destruction of available work or energy will be minimum when entropy generation is minimum according to the Gouy–Stodola theorem [34].

For heat transfer enhancement, the ratio of entropy generation due to heat transfer enhancement to the entropy generation for a non-enhanced device ($N_{s,en}$) is used to characterise the thermodynamic performance.

Where $N_{s,en}$ is the ratio of entropy generation in an enhanced tube to the entropy generation in a plain tube given by

$$N_{s,en} = \frac{(S_{gen})_{en}}{(S_{gen})_p} \tag{14}$$

$N_{s,en}$ should be less than 1 for better thermodynamic performance [34,45–48].

For convection heat transfer problems the entropy generation per unit length (S'_{gen}) was given by Bejan [23] as

$$S'_{gen} = \frac{q'^2}{\pi \lambda T_{bulk}^2 Nu} + \frac{32 \dot{m}^3 c_f}{\pi^2 \rho^2 T_{bulk} D^5} \tag{15}$$

where q' is the heat transfer rate per unit length, $Nu = hD/\lambda$ with $h = q''/(T_w - T_{bulk})$, $c_f = (-dp/dx)\rho D/2G^2$, with $G = 4\dot{m}/\pi D^2$, T_{bulk} is the bulk fluid temperature $(T_{inlet} + T_{outlet})/2$ and D is the diameter of the tube. The first term represents the irreversibility due to heat transfer and the second term the irreversibility due to fluid friction. Eq. (15) provides a means of determining the entropy generation rates in heat transfer and fluid flow problems globally.

According to Kock and Herwig [40], for heat transfer and fluid flow problems involving complex geometries and complex boundary conditions, the analytical method in Eq. (15) gives large deviations compared with a method that determines the local entropy generation in the domain. Therefore, for complex geometries, a method that accounts for the local entropy generation rates is preferred and is more robust [40]. The local entropy generation is determined by combining the heat transfer irreversibility and fluid friction irreversibility according to the following relations [40]:

$$S'''_{gen} = \left(S'''_{gen}\right)_F + \left(S'''_{gen}\right)_H \tag{16}$$

The entropy generation per unit volume due to fluid friction irreversibility $(S'''_{gen})_F$ is given by

$$\left(S'''_{gen}\right)_F = S'''_{PROD,VD} + S'''_{PROD,TD} \tag{17}$$

$S'''_{PROD,VD}$ is the term representing entropy production by direct dissipation and is given by

$$S'''_{PROD,VD} = \frac{\mu}{T}\left(\frac{\partial u_i}{\partial x_j} + \frac{\partial u_j}{\partial x_i}\right)\frac{\partial u_i}{\partial x_j} \tag{18}$$

And $S'''_{PROD,TD}$ represents entropy production by indirect or turbulent dissipation and is given by

$$S'''_{PROD,TD} = \frac{\rho \varepsilon}{T} \tag{19}$$

The entropy generation per unit volume due to heat transfer irreversibility is given by

$$\left(S'''_{gen}\right)_H = S'''_{PROD,T} + S'''_{PROD,TG} \tag{20}$$

where $S'''_{PROD,T}$ is the term representing entropy production by heat transfer with mean temperatures and is given by

$$S'''_{PROD,T} = \frac{\lambda}{T^2}(\nabla T)^2 \tag{21}$$

And $S'''_{PROD,TG}$ is the entropy production by heat transfer with fluctuating temperatures given by

$$S'''_{PROD,TG} = \frac{\alpha_t}{\alpha}\frac{\lambda}{T^2}(\nabla T)^2 \tag{22}$$

In Eq. (22), α and α_t are the viscous and turbulent thermal diffusivities respectively.

For a fluid element of volume V, the entropy generation rate is obtained as the volume integral of the entropy generation rate per unit volume according to:

$$S_{gen} = \iiint_V S'''_{gen}\, dV \tag{23}$$

The local entropy generation rates given by Eqs. (16)–(22), were obtained in the post processing stage of our CFD simulation. The validation of the entropy generation model was done in our earlier study [44] and will not be presented again.

3.3. Boundary conditions

The boundary conditions used include: (1) The outer wall of the absorber tube receives a non-uniform heat flux. The heat flux distribution used in this study is shown in Fig. 3 as determined using ray tracing in SolTrace [49]. For this study, the rim angle (φ_r) used was 80° and the aperture width was 6 m. The receiver angle θ, is the receiver's circumferential angle shown in Fig. 2(a), it is 90° along the positive y-axis and −90° (or 270°) along the negative y-axis. A Direct normal irradiance (DNI) of 1000 W m^{-2} was assumed. (2) Periodic boundary conditions are used for the absorber tube's inlet and outlet. (3) The inner absorber tube walls are considered no-slip and no-penetration. (4) The average glass cover temperature used with the radiation boundary condition was determined separately at each fluid temperature and Reynolds number. A full receiver model without inserts was used for this purpose. The outer wall of the glass cover in this receiver model has a mixed boundary condition to account for both radiation and convection heat transfer. For radiation from the receiver, the receiver exchanges heat with a larger enclosure, the sky. The sky temperature is determined as a function of the ambient temperature from Swinbank [50].

$$T_{sky} = 0.0552\, T_{amb}^{1.5} \tag{24}$$

The ambient temperature used for the full receiver model was 300 K. The convention heat transfer coefficient used for the
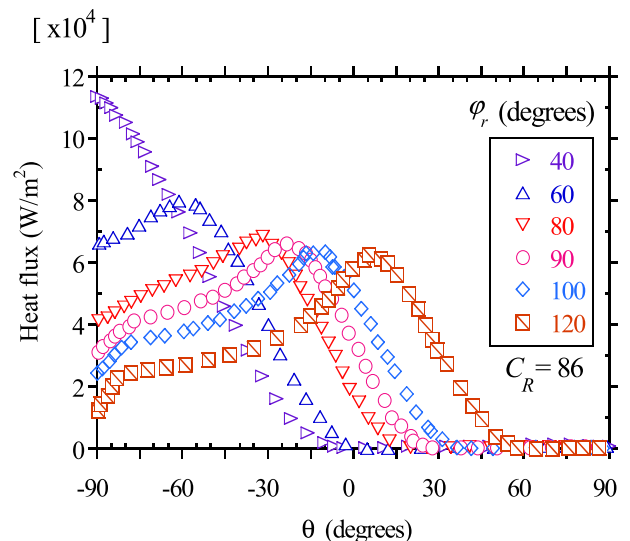

Fig. 3. Heat flux on the receiver's absorber tube as a function of absorber tube circumferential angle and collector rim angle.

convection boundary condition was assumed uniform and is given by Ref. [51].

$$h_w = V_w^{0.58} d_{go}^{-0.42} \qquad (25)$$

where V_w is the wind speed, taken as 2 m s^{-1} in this study and d_{go} is the glass cover outer diameter. For this study, the geometric concentration ratio, C_R is defined as $C_R = A_c/A_r = W_a/d_{ro}$, where A_a is the projected area of the collector's aperture, A_r is the projected area of the absorber tube. W_a is the collector aperture width and d_{ro} is the outer diameter of the receiver's absorber tube.

3.4. Solution procedure

The numerical solution was implemented using a commercial software package ANSYS® release 14.5. The governing equations together with the boundary conditions were solved using a finite-volume approach implemented in a computational fluid dynamics code ANSYS FLUENT [37]. The computational domain was discretised using hexahedral elements with structured elements in the wall normal directions. The coupling of pressure and velocity and was done with the SIMPLE algorithm [52]. Second-order up-wind schemes were employed for integrating the governing equations together with the boundary conditions over the computational domain. To capture the high resolution of gradients in the near wall regions, the y^+ value of about 1 was ensured for all simulations. The enhanced wall treatment [37] was used for modeling the near-wall regions. Where $y^+ = y\mu_\tau/\nu$, ν is the fluid's kinematic viscosity, y is the distance from the wall, and u_τ is the friction velocity given by $\mu_\tau = \sqrt{\tau_w/\rho}$. The solution was considered converged when the scaled residuals of continuity, momentum, turbulence kinetic energy, turbulent dissipation rate and energy ceased changing after about 100 successive iterations. At convergence, the values of the scaled residuals were in the order of less than 10^{-4} for the continuity equation, less than 10^{-6} for velocity, turbulent kinetic energy and turbulent dissipation rate and less than 10^{-7} for energy.

The heat transfer fluid used was SYLTHERM800 [53]. Its thermophysical properties were evaluated at 400 K, 500 K and 600 K as shown in Table 2, as derived from the product's technical data [53]. Stainless steel was used as the absorber tube material. The emissivity of the absorber tube depends on temperature according to Ref. [54].

$$\xi = 0.000327(T + 273.15) - 0.065971. \qquad (26)$$

where T is the absorber tube temperature in degrees Celsius

Grid dependence tests were carried out for representative cases at every Reynolds numbers considered in the study. The solution was considered grid independent when the maximum changes in Nusselt number, friction factor and entropy generation were less than 1% as the mesh element size was changed. The sample grid dependence studies are shown in Table 3. The indices i and $i + 1$ indicate the mesh before and after refinement respectively. The sample mesh is shown in Fig. 4. Generally the number of elements will depend on the length of the periodic module (2H). The number

Table 2
Heat transfer fluid properties [53].

	$T_f = 400$ K	$T_f = 500$ K	$T_f = 600$ K
Density (kg m^{-3})	840	746	638
Viscosity (Pa s)	0.002164	0.000816	0.000386
Thermal conductivity (W m^{-1} K^{-1})	0.1148	0.0958	0.0770
Specific heat capacity (J kg^{-1} K^{-1})	1791.64	1964.47	2135.30

Table 3
Sample grid dependence studies.

Mesh elements	f	Nu	S'_{gen}	$\left\|\frac{f^{i+1}-f^i}{f^{i+1}}\right\|$	$\left\|\frac{Nu^{i+1}-Nu^i}{Nu^{i+1}}\right\|$	$\left\|\frac{S_{gen}^{i+1}-S_{gen}^i}{S_{gen}^{i+1}}\right\|$
$\bar{y} = 0.5$ and $\bar{w} = 0.91$, $Re_p = 1.02 \times 10^4$, $T_{inlet} = 400$ K						
75 761	0.3214	306.7	2.322	–	–	
122 302	0.3213	315.4	2.243	0.000	0.028	0.040
204 723	0.3213	318.2	2.245	0.000	0.009	0.002
$\bar{y} = 0.5$ and $\bar{w} = 0.91$, $Re_p = 1.42 \times 10^5$, $T_{inlet} = 500$ K						
82 500	0.1660	6852.5	2.350	–	–	
156 024	0.1644	6882.4	2.397	0.001	0.004	0.02
268 916	0.1639	6900.1	2.406	0.003	0.003	0.004

of mesh elements used in this study was between 122 300 and 356 000.

3.5. Data reduction

The results from our numerical analysis are presented using the following parameters: The average heat transfer coefficient is given by

$$h = \frac{q''}{T_{ri} - T_{bulk}} \qquad (27)$$

T_{ri} is average inner wall temperature of the absorber tube and T_{bulk} represents the bulk temperature of the fluid at the periodic boundaries.

The average Nusselt number is given by

$$Nu = h\frac{d_{ri}}{\lambda} \qquad (28)$$

where, λ is the thermal conductivity of the heat transfer fluid.

The Reynolds number of flow for both the enhanced absorber tube and non-enhanced absorber tube is defined as

$$Re = \frac{u_m \cdot d_{ri}}{\nu} \qquad (29)$$

In which, ν is the kinematic coefficient of viscosity of the heat transfer fluid and u_m is the mean velocity of the fluid in the tube. Two Reynolds numbers are defined: Re_p is the Reynolds number based on plain absorber tube mean velocity and Re_{en} is the Reynolds number based on the mean velocity of the tube with twisted tape inserts. For the same mass flow rate, the mean velocity and thus the Reynolds number in an absorber tube with twisted tape is higher due to fluid acceleration.

The friction factor is defined as

$$f = \frac{\Delta P}{\frac{1}{2}\rho \cdot u_m^2 \cdot \frac{L}{d_{ri}}} \qquad (30)$$

For a smooth tubes the value of the friction factor (f) can be obtained for different Reynolds numbers according to the Petukhov's correlation given in Ref. [55] as

$$f = (0.790 \ln Re - 1.64)^{-2} \qquad (31)$$

whereas the average Nusselt number is given according to Gnielinski's correlation [55] for both low and high Reynolds numbers as

$$Nu = \frac{(f/8)(Re - 1\,000)Pr}{1 + 12.7(f/8)^{0.5}(Pr^{2/3} - 1)} \qquad (32)$$

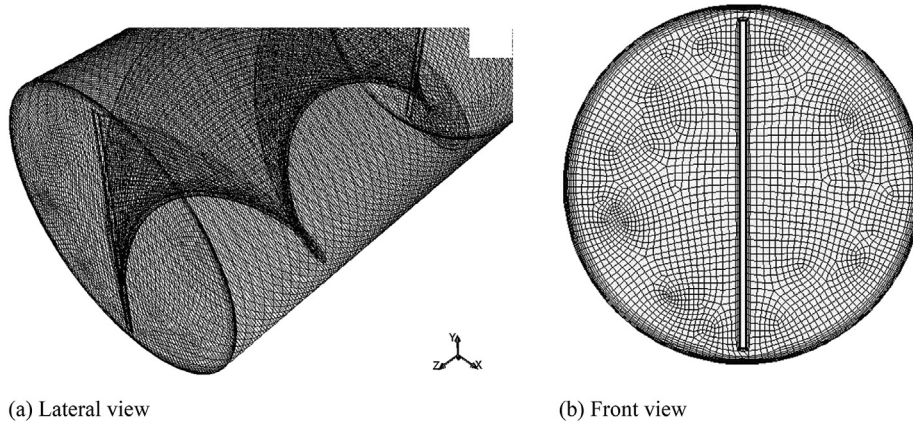(a) Lateral view   (b) Front view

Fig. 4. Sample mesh of the receiver's absorber tube used in this study.

For $0.5 \leq Pr \leq 2000$ and $3 \times 10^3 \leq Re \leq 5 \times 10^6$.

The absorber tube's circumferential temperature difference is given as the difference between the maximum and minimum temperatures of the absorber tube according to

$$\phi = T_{r,\max} - T_{r,\min} \tag{33}$$

The thermal enhancement factor χ for evaluating thermal performance at constant pumping is defined as [8].

$$\chi = \left(Nu/Nu_p\right)\Big/\left(f\Big/f_p\right)^{(1/3)} \tag{34}$$

4. Results and discussions

4.1. Validation of numerical results

Our numerical results were validated in several steps. First, we validated the parabolic trough receiver model using experimental data from Dudley et al. [36]. As shown in Fig. 5, good agreement was obtained for temperature gain and collector efficiency. From a comparison of different turbulence models, the realisable $k-\varepsilon$ model was shown to give results of the local Nusselt number on the absorber tube circumference close to the Reynolds stress model as shown in Fig. 6. Though more accurate than the realisable $k-\varepsilon$, the Reynolds stress model is computationally expensive and was

therefore not used in this study. For heat transfer enhancement using twisted tape inserts, our twisted tape numerical model was compared with correlations put forward by Manglik and Bergles [56]. As shown in Fig. 7(a) and (b), good agreement was obtained for both Nusselt numbers and friction factor respectively. Nusselt numbers are within ±6.5% and friction factors are with in ±8%.

4.2. Temperature difference in a receiver with a plain absorber tube

With no heat transfer enhancement, Fig. 8 shows that as the concentration ratios increase, the absorber tube's circumferential temperature difference also increases. In this figure the inlet temperature used is 350 K. At a Reynolds number of 1.94×10^4, the absorber tube circumferential temperature differences are 92 °C, 115 °C, 138 °C, 159 °C and 183 °C, 204 °C and 227 °C at concentration ratios 57, 75, 86, 100, 114, 128 and 143 respectively. The increase in the concentration ratio results in higher peak heat fluxes on the absorber tube. The figure further shows a reduction of absorber tube's circumferential temperature difference with increasing Reynolds numbers. Therefore, as the concentration ratios increase, higher flow rates become necessary to reduce the temperature difference in the absorber tube. Heat transfer enhancement is the
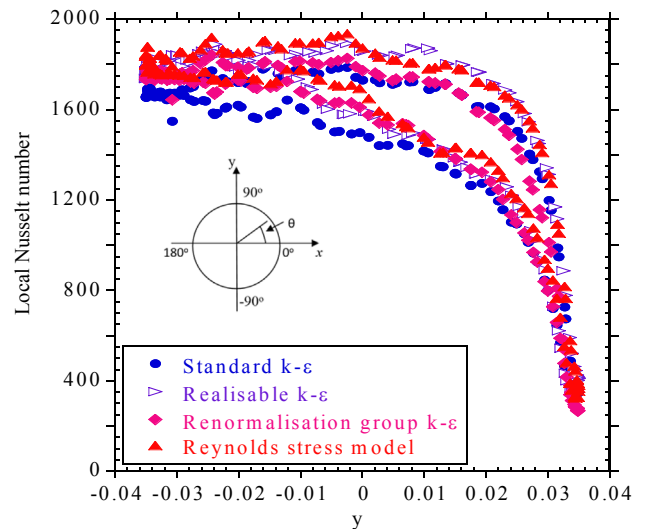

Fig. 5. Validation of the parabolic trough receiver temperature gain and thermal efficiency.

Fig. 6. Comparison of local Nusselt number around absorber tube circumference for different turbulence models with a twisted tape insert of $\bar{y} = 0.5$, $\bar{w} = 0.71$, inlet temperature of $T_{inlet} = 500$ K and $Re_p = 112\,000$.
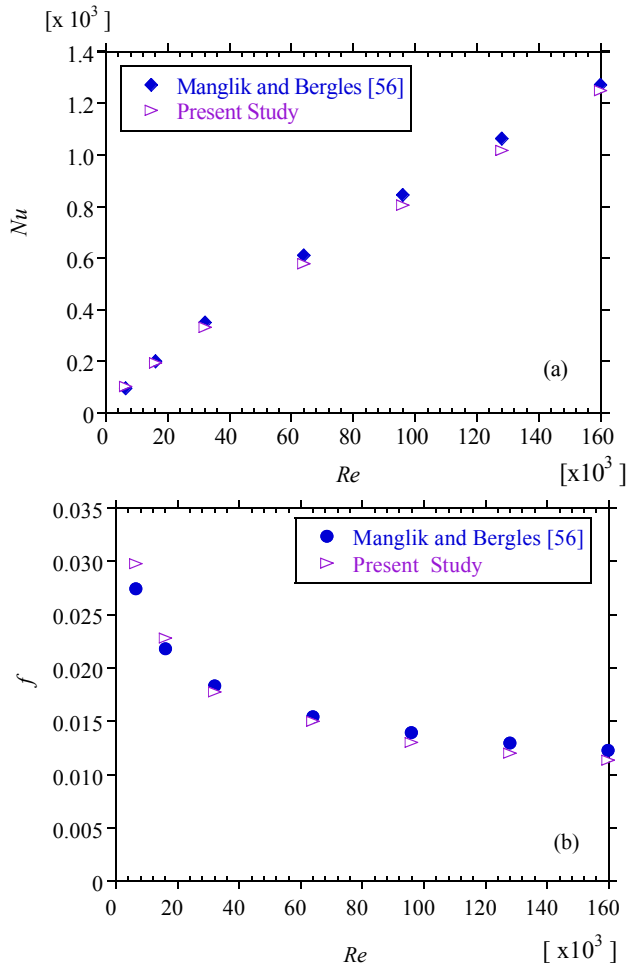
Fig. 7. Validation of twisted tape model: (a) Heat transfer as a function of Reynolds number, (b) Fluid friction as a function of Reynolds number.

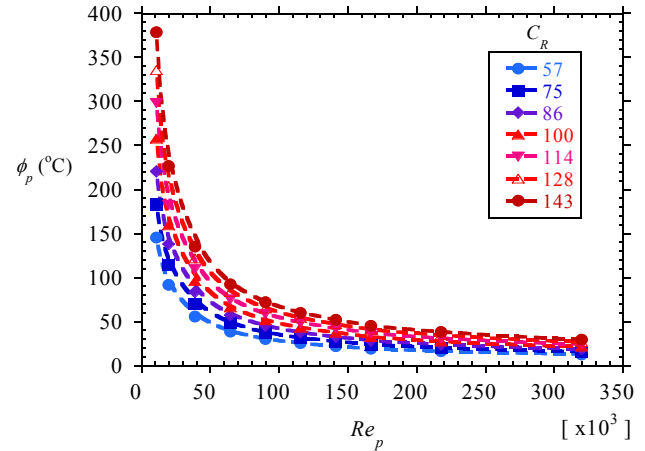**Fig. 8.** Absorber tube's circumferential temperature difference as a function of Reynolds number and concentration ratio at $T_{inlet} = 350$ K.

other option to improve the receiver's performance and reduce absorber tube's circumferential temperature difference. With heat transfer enhancement, lower flow rates can be used ensuring higher collector field outlet temperatures while reducing the absorber tube circumferential temperature differences.

4.3. Flow structure

4.3.1. Velocity field

The velocity contours of the flow field in the absorber tube with twisted tape inserts are shown in Fig. 9(a)–(e) at different stream wise locations for a twisted tape with $\tilde{y} = 1.0$ ($2H = 0.132$ m) and $\tilde{w} = 0.75$ with $Re_p = 150\,300$ and $T_{inlet} = 500$ K. As shown in the figures, the use of twisted tape inserts generates vortices around the tape in the core flow area. The presence of these vortices helps in disrupting the boundary layer as well as in enabling mixing of the fluid from the heated lower half of the absorber tube with the fluid from the upper half of the absorber tube receiving only direct solar radiation. This boundary layer disruption and fluid mixing leads to improved heat transfer performance as well as reduction of absorber tube circumferential temperature gradients. Fig. 10(a) shows the velocity vectors in the absorber tube with twisted tape inserts. It is also clear that the fluid around the twisted tape insert is accelerated. Fig. 10(b) shows the streamlines through the absorber tube with twisted tape inserts. As shown in this figure, twisted tape

inserts induce swirl flow in the absorber tube. The resulting helical path means that the fluid takes longer in the tube compared to when there are no twisted tape inserts, this results in increased fluid agitation, thus improved heat transfer performance. In Fig. 9(a) and (e), it can be seen that the velocity profile at the inlet is the same as that at the outlet as expected since the flow is periodically fully developed.

4.3.2. Temperature field

From the flow field discussed in Section 4.3.1, the use of twisted tape inserts promotes fluid mixing and thus influences the temperature distribution in the absorber tube. As shown in Fig. 11(a)–(e), there is improved temperature distribution in the absorber tube due to the use of twisted tape inserts. Compared to an absorber tube with no inserts as shown in Fig. 11(f), a more uniform temperature distribution is obtainable with the use of twisted tape inserts. Also as the figure shows, the temperature profiles at the inlet and outlet are similar implying thermally fully developed flow. It is this tendency of twisted tape inserts to give a uniform temperature distribution in the receiver's absorber tube thus reducing the thermal boundary layer thickness that that leads to improved heat transfer performance and subsequently reduced circumferential temperature differences in the receiver tube.

4.4. Heat transfer

Fig. 12(a) and (b) shows the variation of the local Nusselt number on the absorber tube wall in the longitudinal direction and along the tube's circumference at different stream wise locations respectively, for $T_{inlet} = 500$ K, $\tilde{y} = 0.5$, $\tilde{w} = 0.71$ and $Re_p = 112\,000$. As shown, the local Nusselt number varies significantly around the tube's circumference owing to the non-uniform heat flux received by the receiver tube as well as the flow structure in the tube. For a given longitudinal line on the absorber tube's wall, the local Nusselt number does not vary significantly when compared to the variation around the tube's circumference as shown in Fig. 12(a). However, a closer look at each line reveals variation in the local Nusselt number along the tubes longitudinal direction due to the swirling nature of flow induced by the twisted tape. The presence of peaks with high Nusselt number indicates areas of high heat transfer due to fluid bouncing from the tape and impinging on tube walls. The different heat flux and thus the resulting wall temperatures on the absorber tube give different local Nusselt numbers around the tube's circumference. The low local Nusselt number at the top of the
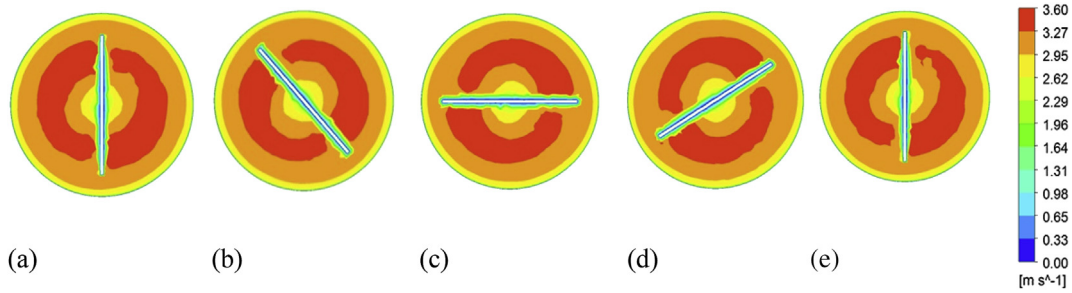
Fig. 9. Velocity contours in the absorber tube with a twisted tape insert for $Re_p = 150\ 300$, $T_{inlet} = 500$ K, $\bar{y} = 1.0$ and $\bar{w} = 0.75$: (a) z = 0 m (inlet), (b) z = 0.030 m, (c) z = 0.066 m, (d) z = 0.090 m, and (e) z = 0.132 m (outlet).
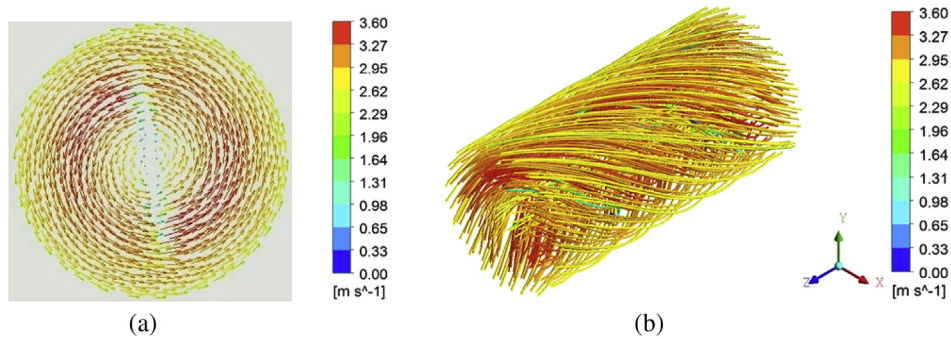

Fig. 10. Velocity field in the absorber tube with twisted tape inserts for $Re_p = 150\ 300$, $T_{inlet} = 500$ K, $\bar{y} = 1.0$ and $\bar{w} = 0.75$: (a) velocity vectors, and (b) streamlines.

absorber tube's circumference, $\theta = 90°$ is due to the low heat flux received by the receiver and the high Nusselt numbers on the lower half of the tube are due to the concentrated heat flux received there as was shown in Fig. 3. The local Nusselt number at $\theta = 180°$ is higher than the local Nusselt number at $\theta = 0°$ despite the two having the same heat flux given the symmetrical nature of the heat flux received on the receiver. This might be due to high flow impingement on the left half of the absorber tube ($90° \leq \theta \leq 180°$ and $180° \leq \theta \leq 90°$) compared to that the right half ($-90° \leq \theta \leq 0°$ and $180° \leq \theta \leq 90°$).

The heat transfer performance can be given using the average Nusselt numbers. Fig. 13(a)–(c) shows the heat transfer performance of the receiver tube with twisted tape inserts at different twist ratios and width ratio for 400 K, 500 K and 600 K respectively. As expected, the average Nusselt numbers increase as the twist ratio reduces due to the increase in the helical tube length the fluid must cover, increased fluid mixing and increased turbulent intensity. The same variation of the average Nusselt number with Reynolds number is shown to exist at the different fluid temperatures considered. At higher fluid temperatures, the Reynolds numbers are higher due to lower fluid density and lower viscosity at the corresponding flow rates. Thus, the heat transfer performance at higher temperatures is shown to be higher for the corresponding flow rates. The variation of the average Nusselt number with width ratio can be clearly shown at a specific Reynolds number. In Fig. 14, the variation of the average Nusselt number with
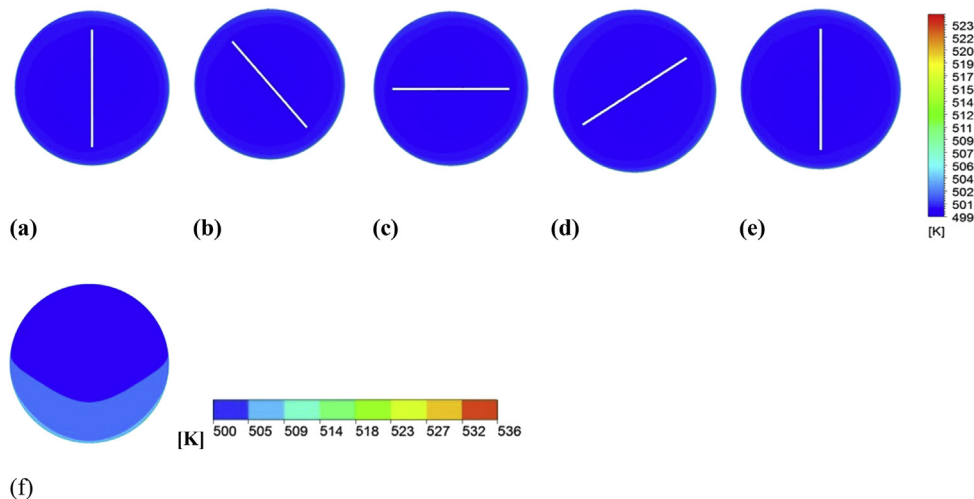

Fig. 11. Temperature contours at different stream wise locations in the absorber tube at $T_{inlet} = 500$ K, $Re_p = 150\ 300$ for $\bar{y} = 1.0$ and $\bar{w} = 0.75$ at (a) z = 0 m (inlet), (b) z = 0.030 m, (c) z = 0.066 m, (d) z = 0.090 m, (e) z = 0.132 m (outlet) and for (f) an absorber tube without inserts.
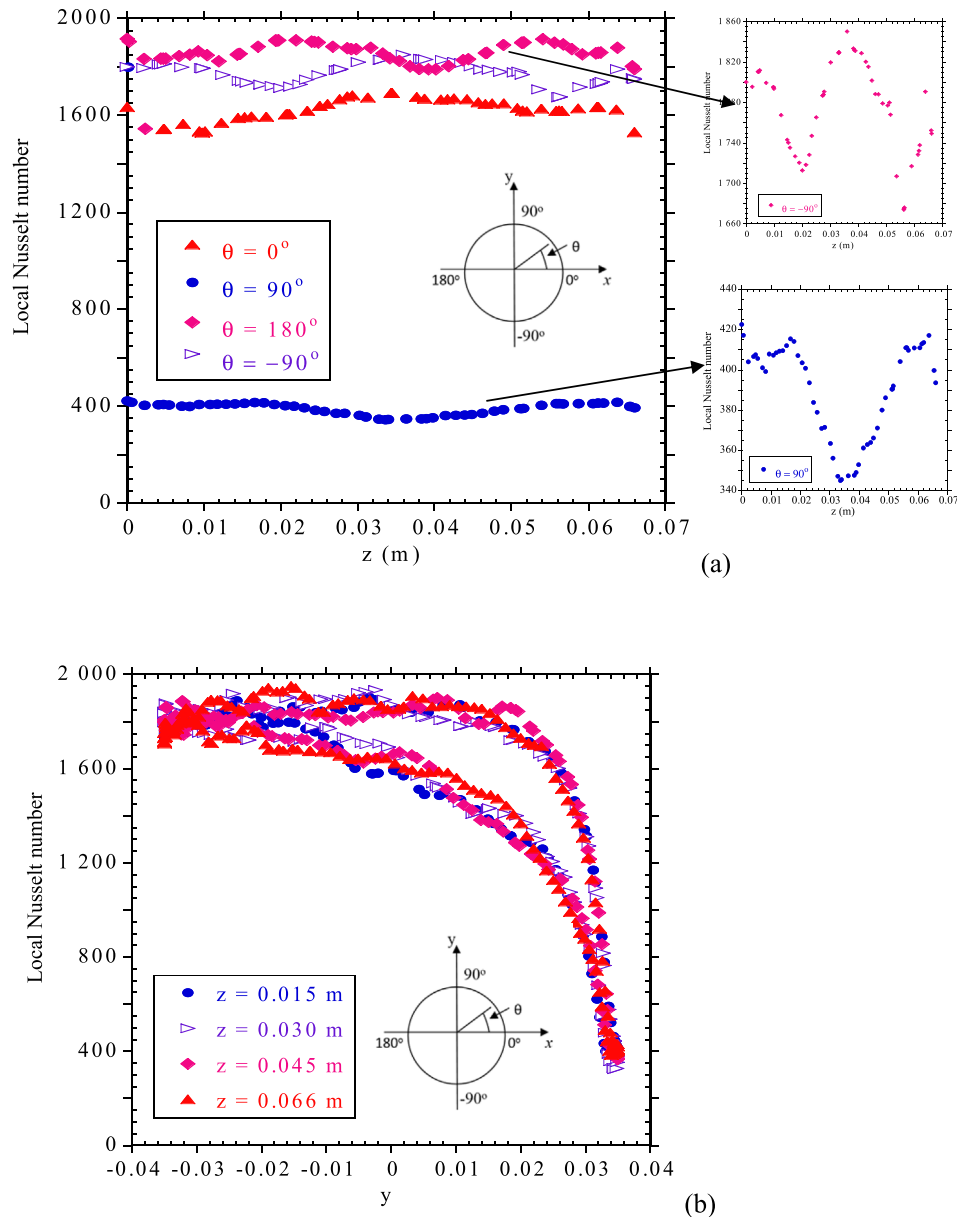
Fig. 12. Local Nusselt number for $\bar{y} = 0.5$, $\bar{w} = 0.71$, $T_{inlet} = 500$ K and $Re_p = 112\,000$ (a) as a function of stream wise length along the tube, and (b) along the absorber tube's circumference at different stream wise locations.

width ratio is shown for a Reynolds number (Re_p) of 8.13×10^4 and an inlet temperature of 600 K. The average Nusselt number is shown to increase as the width ratio increases, with significant increments shown at low values of the twist ratio. At lower twist ratios the fluid's path is longer and thus sufficient mixing results in improved heat transfer performance.

The heat transfer enhancement achieved due to the use of twisted tape inserts in the receiver's absorber tube depends on the twist ratio, width ratio and Reynolds number. For the range of parameters considered the average Nusselt number increases by 1.05–2.69 times compared with a receiver with a plain absorber tube.

The improved heat transfer performance is expected to reduce the absorber tube's circumferential temperature difference. Therefore, the variation of the absorber tube's circumferential temperature difference with twist ratio, width ratio and Reynolds number is an inverse of the average Nusselt number variation. As

shown in Fig. 15(a)–(c), the circumferential temperature differences in the absorber tube reduce with increasing Reynolds numbers, increasing twisted tape width ratio and reducing twisted tape twist ratio. The absorber tube's circumferential temperature differences are shown to reduce by between 4 and 68% when compared with a receiver with a plain absorber tube for the range of parameters considered. As shown in Fig. 15(a)–(c), heat transfer enhancement is crucial at low Reynolds numbers and low fluid temperatures since absorber tube circumferential temperature differences are large at these conditions.

4.5. Friction factor

Most heat transfer enhancement techniques will provide improved heat transfer performance but with additional fluid friction penalty. For this study, the variation of fluid friction with Reynolds numbers, twist ratio and width ratio is shown in
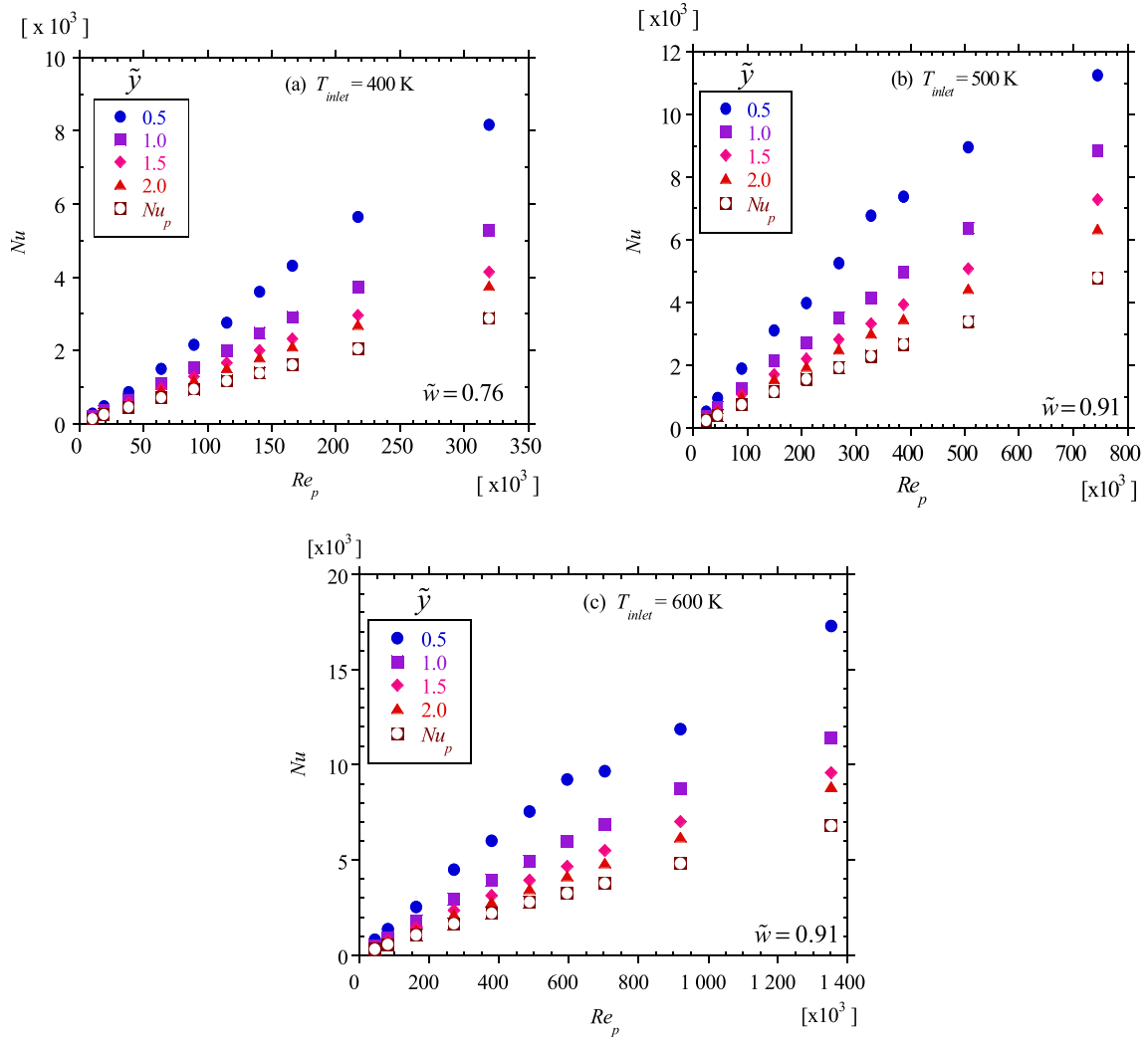
Fig. 13. Average Nusselt number as a function of Reynolds number at different twist ratios for (a) T_{inlet} = 400 K and $\bar{w}$ = 0.76, (b) T_{inlet} = 500 K and $\bar{w}$ = 0.91 and (c) T_{inlet} = 600 K and $\bar{w}$ = 0.91.
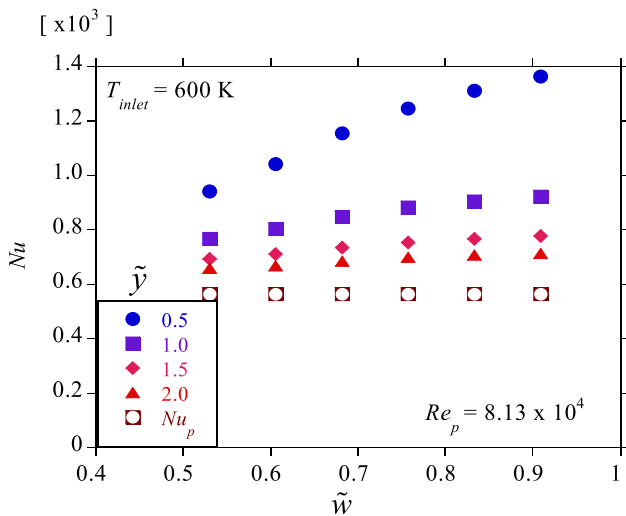

Fig. 14. Average Nusselt number as a function of width ratio and twist ratio for Re_p = 8.13 × 10⁴ and T_{inlet} = 600 K.

Fig. 16(a)–(c) for width ratios of 0.76 and fluid temperature 400 K, 0.83 and fluid temperature 400 K and width ratio 0.91 and fluid temperature 600 K respectively. As expected the friction factors increase with reducing Reynolds number, reducing twist ratios and increasing width ratios. The increase in fluid friction is due to an increase in flow resistance as a result of swirl flow, impingement on the absorber tube as well as obstruction to flow by the twisted tape insert. The friction factors increase between 1.60 and 14.5 times compared with a receiver with a plain absorber tube for the range of parameters considered.

4.6. Thermal performance evaluation

As a preliminary tool for comparison of heat transfer enhancement techniques at constant pumping power, the thermal enhancement factor, χ given by Eq. (34) was used. Enhancement techniques with χ > 1 are considered effective heat transfer enhancement techniques when pumping power is a concern. Fig. 17(a) and (b) shows the variation of the thermal enhancement factor with Reynolds number at different twist ratios. Generally, the thermal enhancement factor increased with Reynolds numbers at a given twist ratio. This trend was also presented in a study by Cheng et al. [16]. The increasing trend of the thermal enhancement factor
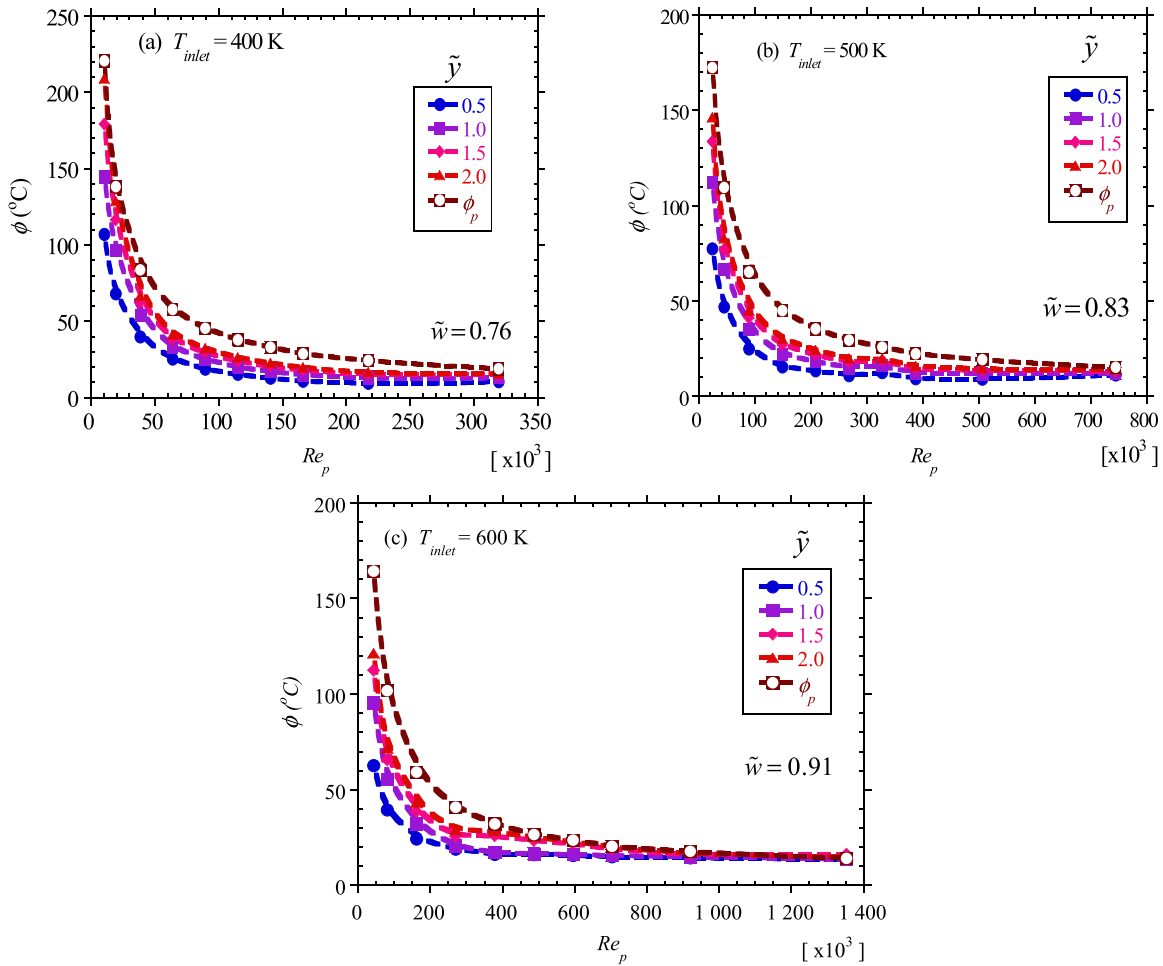
Fig. 15. Absorber tube's circumferential temperature difference as a function of Reynolds number and twist ratio for (a) $T_{inlet} = 400$ K and $\bar{w} = 0.76$, (b) $T_{inlet} = 500$ K and $\bar{w} = 0.83$ and (c) $T_{inlet} = 600$ K and $\bar{w} = 0.91$.

could be due to the higher heat transfer performance as a result of intense fluid mixing as Reynolds numbers increase. The high temperature fluid in the lower half of the receiver's absorber tube is displaced and replaced with low temperature fluid from the upper half of the tube leading to more heat transfer to the now low temperature fluid. For the range of parameters considered, the thermal enhancement factor was in the range $0.74 \leq \chi \leq 1.27$.

To show the actual influence of heat transfer enhancement on the thermal performance of the parabolic trough receiver, the thermal efficiency that takes into account the increase in fluid friction with the use of inserts is considered. With this, the reduction in radiation heat loss resulting from reduced absorber tube temperatures is also accounted for. Accordingly, the thermal efficiency is given as:

$$\eta_{th} = \frac{\dot{q}_u - \dot{W}_p / \eta_{el}}{I_b A_c} \qquad (35)$$

The electrical efficiency of the power block η_{el} used in Eq. (35) was taken as 32.7% [57], $\dot{q}_u = \dot{m}c_p(T_{outlet} - T_{inlet})$ and $\dot{W}_p = \dot{V}\Delta P$. It can be observed from Fig. 17(c) and (d) that the thermal efficiency of the collector increases with heat transfer enhancement for some range of Reynolds numbers at every value of twist ratio. Improvements in thermal efficiency in the range 5–10% are achievable for twist ratios $\bar{y}$ greater than 1.0 for almost all width ratios provided that the flow rate is lower than 43 m³ h⁻¹. This flow rate

corresponds to 10.05 kg s⁻¹ at 400 K, 8.94 kg s⁻¹ at 500 K, 7.65 kg s⁻¹ at 600 K and 6.91 kg s⁻¹ at 650 K. At twist ratios lower than 1, the thermal efficiency increases with the use of twisted tape inserts at low Reynolds numbers, but as the Reynolds numbers increase, the pumping power required increases and become larger than the gain in heat transfer rate, so the efficiency becomes lower than one in a collector with a non-enhanced receiver. The highest increase in efficiency will be at the lowest Reynolds numbers, since it is at these low Reynolds numbers that the heat transfer performance is low and the absorber tube's temperatures are higher.

The increase in the efficiency of the collector is due to improved heat transfer performance and the associated reduction in absorber tube temperatures. Heat transfer enhancement will reduce the absorber tube's temperatures. As a result, the emissivity will also reduce since it varies with temperature. This will lead to reduced radiation heat loss. The thermal efficiency of a collector with a non-enhanced receiver tube is shown to increase with Reynolds numbers up to some value, after which it becomes constant. This is because at higher flow rates, the reduction in absorber tube temperatures is not significant as has been shown in the present study.

4.7. Heat transfer and fluid friction correlations

Based on the results from our numerical investigation, correlations for Nusselt number and friction factor were derived using regression analysis.
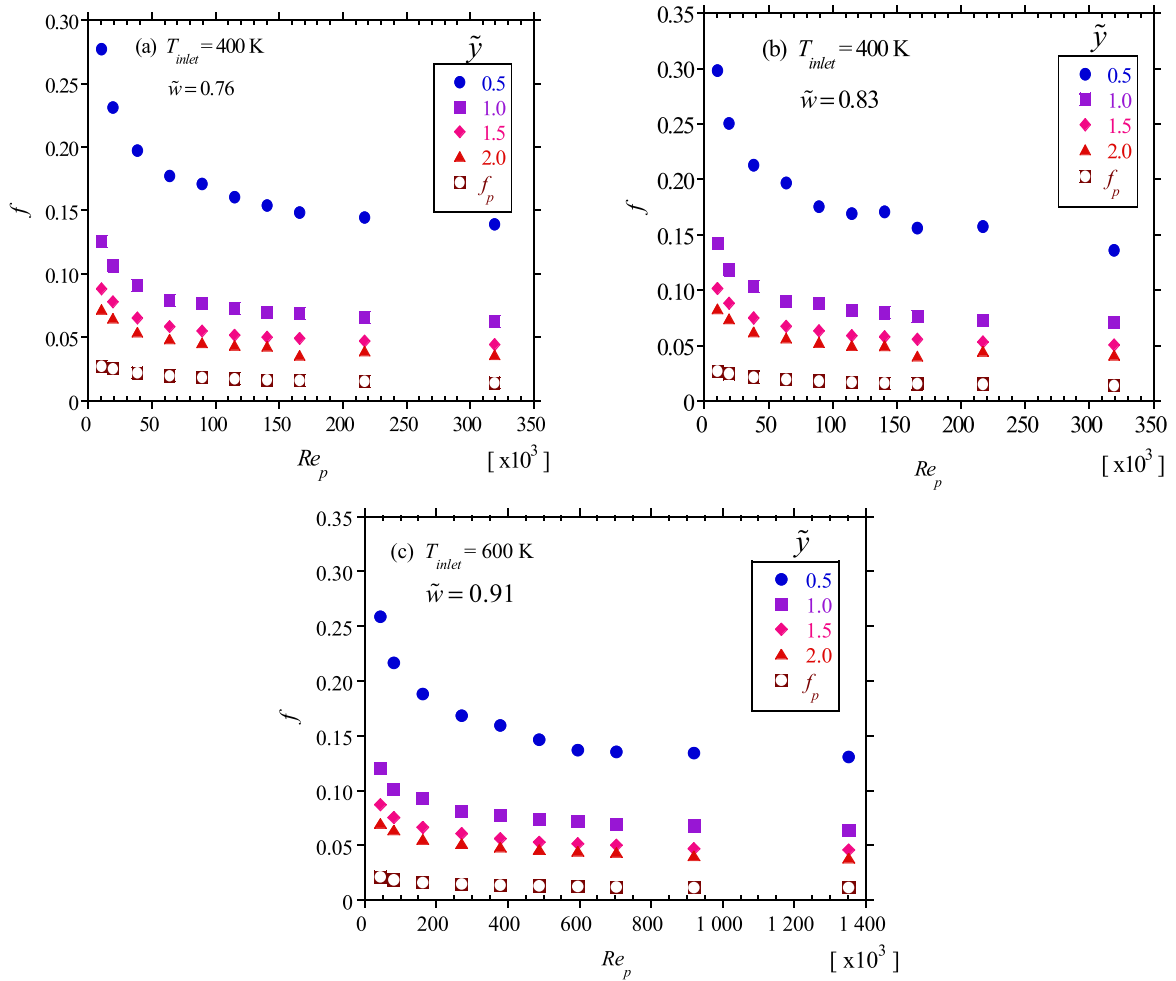
Fig. 16. Friction factor as a function of Reynolds number and twist ratio for (a) T_{inlet} = 400 K and $\bar{w}$ = 0.76, (b) T_{inlet} = 400 K and $\bar{w}$ = 0.83 and (c) T_{inlet} = 600 K and $\bar{w}$ = 0.91.

The Nusselt numbers are correlated by:

$$Nu = 0.01709 Re_p^{0.8933} Pr^{0.3890} \tilde{y}^{-0.4802} \tilde{w}^{0.3881} \qquad (36)$$

Valid for $1.02 \times 10^4 \leq Re_p \leq 1.35 \times 10^6$ and $10.7 \leq Pr \leq 33.7$
$\qquad$ $400\,K \leq T \leq 600\,K$
$\qquad$ $0.53 \leq \tilde{w} \leq 0.91$
$\qquad$ $0.50 \leq \tilde{y} \leq 2.0$

Correlations in Eq. (36) is valid within $\pm 15\%$ as shown in the parity plot for the observed Nusselt numbers and those predicted from the correlations for 360 design points in Fig. 18.

The friction factors are correlated by

$$f = 1.1289 \tilde{y}^{-1.0917} \tilde{w}^{1.1802} Re_{en}^{-0.1923} \qquad (37)$$

Valid for $1.02 \times 10^4 \leq Re \leq 1.35 \times 10^6$ and $10.7 \leq Pr \leq 33.7$
$\qquad$ $400\,K \leq T \leq 600\,K$
$\qquad$ $0.53 \leq \tilde{w} \leq 0.91$
$\qquad$ $0.50 \leq \tilde{y} \leq 2.0$

Eq. (37) predicts the friction factors with in $\pm 14\%$ for the entire range of Reynolds numbers and parameter considered in this study. Fig. 19 shows the parity plot for the friction factors.

In Eqs. (36) and (37), Re_p and Re_{en} are Reynolds number based on the actual mean velocity in the plain and enhanced absorber tube respectively. The mean velocity in the enhanced tube is higher than that in the plain tube due to the vortices generated by the twisted tape. Re_{en} is related to the plain absorber tube Reynolds number (Re_p) according to Eq. (38) for the range of parameters considered.

$$Re_{en} = 1.9681 \tilde{y}^{-0.4048} \tilde{w}^{0.6364} Re_p^{0.9818} \qquad (38)$$

4.8. Entropy generation

Another way of assessing the performance of enhancement techniques is the consideration of the entropy generation rates as a result of applying the enhancement technique [34,46,48]. With this, the aim is to minimise the irreversibilities and the technique with the lowest entropy generation rates is desirable. Further, enhancement techniques with the entropy generation ratio, $N_{s,en}$ less than 1 makes thermodynamic sense. In this section, results of entropy generation analysis for a parabolic trough receiver with twisted tape inserts are presented.

4.8.1. Heat transfer and fluid flow irreversibilities

Heat transfer and fluid flow irreversibilities are the two irreversibilities present in convection heat transfer problems. For heat
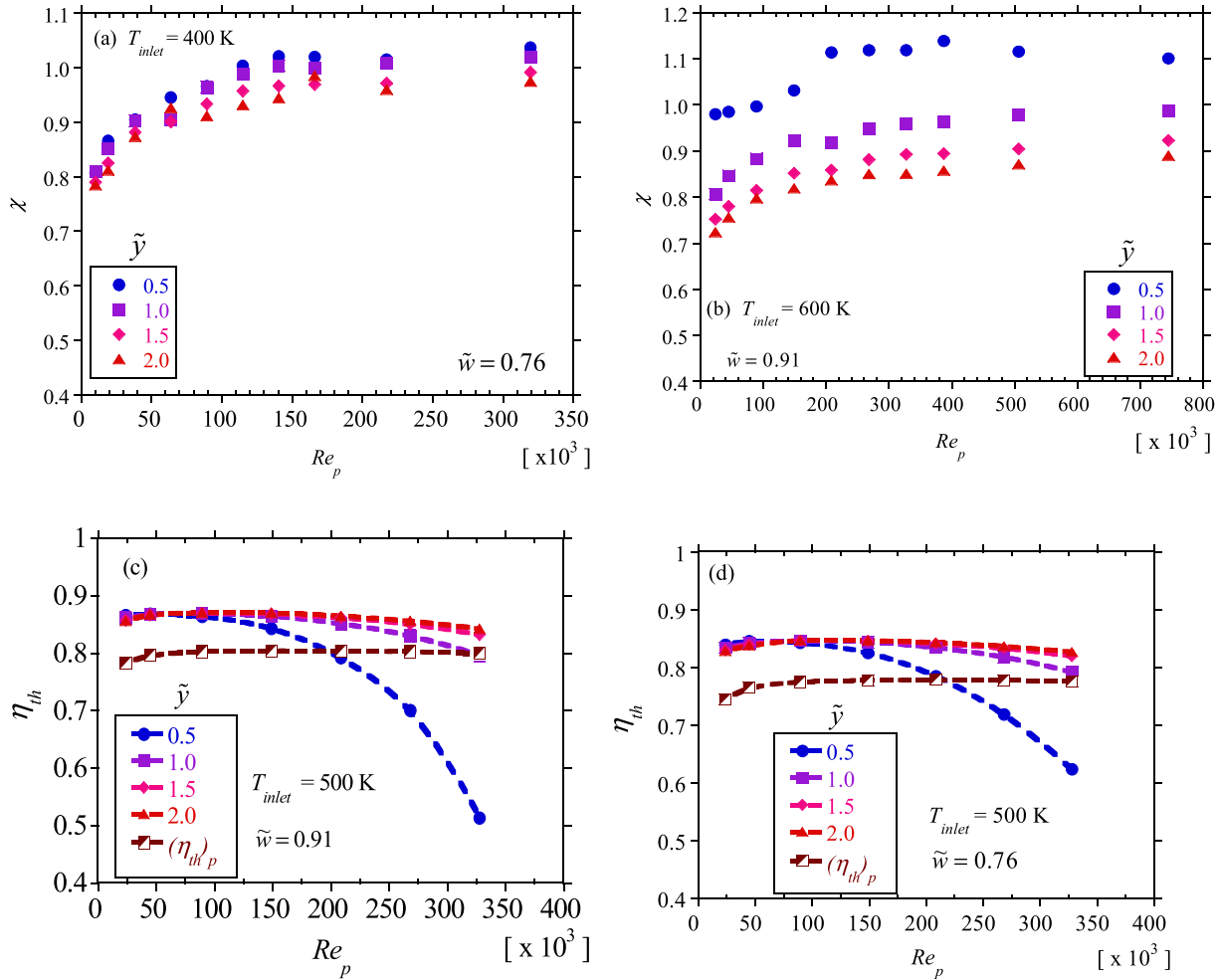
Fig. 17. Thermal performance evaluation: (a) Thermal enhancement factor as a function of Reynolds number and twist ratios for $T_{inlet} = 400$ K and $\bar{w} = 0.76$, (b) Thermal enhancement factor as a function of Reynolds number and twist ratios for $T_{inlet} = 600$ K and $\bar{w} = 0.91$, (c) Thermal efficiency as a function of Reynolds number and twist ratio for $T_{inlet} = 500$ K and $\bar{w} = 0.91$ and (d) Thermal efficiency as a function of Reynolds number and twist ratio for $T_{inlet} = 500$ K and $\bar{w} = 0.76$.

transfer enhancement, the objective is to minimise the heat transfer irreversibility. But as the heat transfer irreversibility is reduced, the fluid flow irreversibility will increase. Fig. 20 shows the variation of the heat transfer irreversibility, fluid friction

Fig. 18. Nusselt number parity plot.

irreversibility and the total entropy generation rate at the smallest and largest twist ratios for a width ratio of 0.91. Generally, the heat transfer irreversibility decreases with increasing Reynolds numbers and decreasing twist ratios while the fluid friction irreversibility increases with increasing Reynolds numbers and decreasing twist ratios. The figure shows existence of an optimal Reynolds number for which the total entropy generation (S'_{gen}) is a minimum. The optimal Reynolds number is shown to be low at tight twist ratios and high at less tight twist ratios.

Fig. 21(a) and (b) shows clearly the variation of the fluid friction and heat transfer irreversibility irreversibilities respectively, with Reynolds number at different width ratios for $\tilde{y} = 0.5$. As shown, the fluid friction irreversibility increases significantly with increasing width ratio in all cases as the Reynolds numbers increase. While the heat transfer irreversibility reduces with increasing width ratio and increasing Reynolds number. The same variation is expected at other values of twist ratio.

Fig. 22(a) and (b) depicts the variation of the heat transfer irreversibilities and fluid friction irreversibilities with Reynolds number at different twist ratios. It is also shown that the heat transfer irreversibilities reduce with Reynolds number while the fluid flow irreversibilities increase with Reynolds number. Significant increase of the fluid flow irreversibilities is shown at high Reynolds numbers and low twist ratios. The decrease in the heat transfer irreversibility is mainly due to improved heat transfer
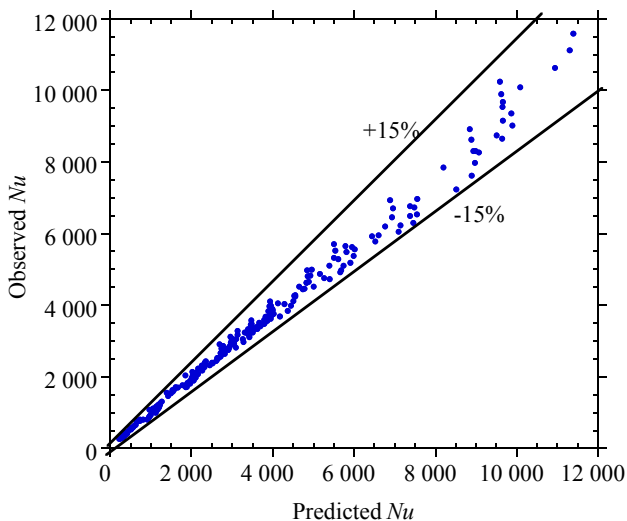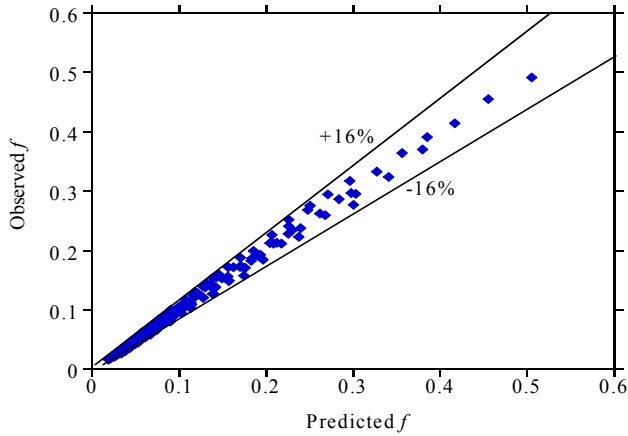
Fig. 19. Friction factor parity plot.

performance and thus reduced finite temperature differences while the increase in fluid friction is mainly due to higher pressure drop. This kind of variation of heat transfer irreversibilities and fluid flow irreversibilities results in minimum entropy generation at some Reynolds number.

4.8.2. Variation of the Bejan number

To show the contributions of each irreversibility to the total entropy generation rate, the Bejan number is usually used. It relates the entropy generation due to heat transfer to the total entropy generation according to:

$$Be = \frac{(S_{gen})_H}{S_{gen}} \tag{39}$$

The Bejan number ranges from $0 \leq Be \leq 1$, the heat transfer irreversibility dominates if Be is close to one while the fluid friction irreversibility dominates if Be is close to zero. Accordingly, the heat transfer enhancement at a given Reynolds number should be considered if Be is closer to 1 than to 0.

Fig. 23(a) and (b) shows the variation of Bejan number with Reynolds number at different twist ratios for $\tilde{w} = 0.91$ and variation of Bejan number with Reynolds number at different width ratios for $\tilde{y} = 0.61$ respectively. The figures show the Bejan number to reduce when compared with the Bejan number of a plain
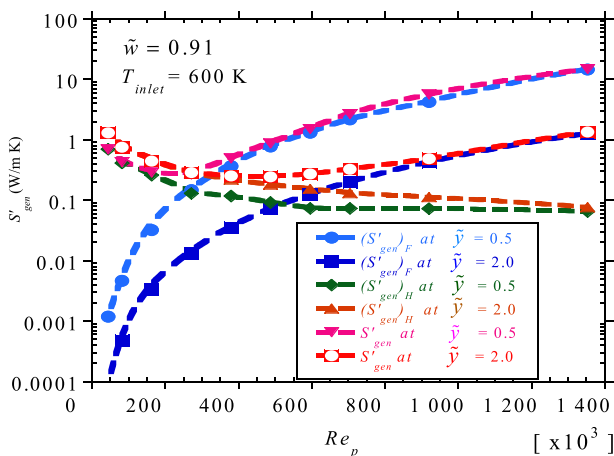

Fig. 20. Entropy generation distribution in the receiver as a function of Reynolds number and twist ratios ($\tilde{y}$) of 0.5 and 2.0 for $T_{inlet} = 600$ K and $\tilde{w} = 0.91$.

absorber tube. At a given Reynolds number, the Bejan number reduces as the twist ratio reduces and as the width ratio increases. This is due to improved heat transfer performance as well as the corresponding increase in fluid friction. The Bejan number is also shown to reduce with an increase in Reynolds number due to reduced heat transfer irreversibility and increasing fluid flow irreversibility as Reynolds numbers increase. The change in the Bejan number is more pronounced as the twist ratio changes.

4.8.3. Total entropy generation rate

The total entropy generation rate is the sum of the heat transfer irreversibility and fluid flow irreversibility. Given, the variation of the fluid flow and heat transfer irreversibilities discussed above, the total entropy generation rate is expected to reduce with Reynolds number up to some minimum value due to reduction in heat transfer irreversibility and then increase with further increase in Reynolds number due to the significant increase in fluid flow irreversibility.

Fig. 24(a) and (b) shows the variation of the total entropy generation rate per unit length of the receiver with Reynolds number at different width ratios. Fig. 24(c) and (d) shows the variation of the total entropy generation rate per unit length with Reynolds number at different twist ratios. The figures show that the optimal Reynolds number depends on both the width ratio and the twist ratio. For low twist ratios, the optimal Reynolds number is low and for large twist ratios the optimal Reynolds number increases. Below the optimal Reynolds number, use of large width ratios or small twist ratios yields low values of entropy generation rate, since the heat transfer irreversibility dominates. Beyond the optimal Reynolds number, large width ratios and small twist ratios yield high entropy generation rates since fluid flow irreversibilities are the dominant source of entropy generation. From the figure, it is clear that the use of high Reynolds numbers and low twist ratios is detrimental to the thermodynamic performance of the receiver, given the associated higher entropy generation rates.

4.8.4. Thermodynamic performance

For evaluation of the thermodynamic effectiveness of a given heat transfer technique, the entropy generation ratio given in Eq. (14) is used. The value of this ratio should be less than 1 if the enhancement technique is thermodynamically feasible. For ratios less than 1.0, the irreversibilities are reduced when compared to a plain tube and for ratios greater than 1, the enhancement techniques results in more irreversibilities compared to a plain tube.

Fig. 25(a) and (b) shows the variation of $N_{s,en}$ with Reynolds number at different twist ratios for 400 K and 500 K and a width ratio of 0.91. Generally, twisted tape inserts are not thermodynamically desirable at high Reynolds numbers. At each twist ratio, a Reynolds number can be obtained at which $N_{s,en}$ is less than 1.0. The value of this Reynolds number increases as the twist ratio increases. For large values of Reynolds numbers, the value of $N_{s,en}$ increases with the increase in the width ratio and reduction in the twist ratio due to the increased contribution of the fluid flow irreversibility to entropy generation. Therefore, at high Reynolds numbers less tight twisted tapes will be desirable since they will result in low values of entropy generation rates but low heat transfer enhancement will be achieved. For Reynolds numbers at which $N_{s,en}$ is less than 1.0, the entropy generation is reduced up to 58.8%.

5. Conclusion

In this study, the use of wall detached twisted tape inserts for heat transfer enhancement in parabolic trough receivers was numerically investigated. The use of twisted tape inserts is shown to significantly improve the receiver's heat transfer performance
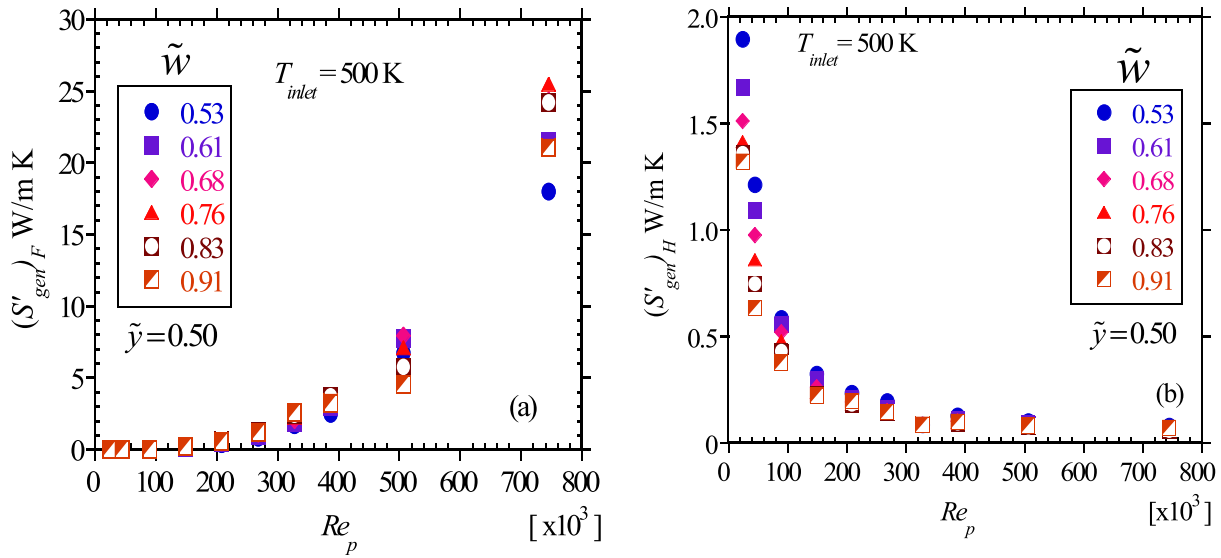
Fig. 21. Entropy generation in the receiver for $T_{inlet} = 500$ K and $\tilde{y} = 0.50$: (a) entropy generation due to fluid flow irreversibilities as a function of Reynolds number and width ratio and (b) entropy generation due to heat transfer irreversibilities as a function of Reynolds number and width ratio.
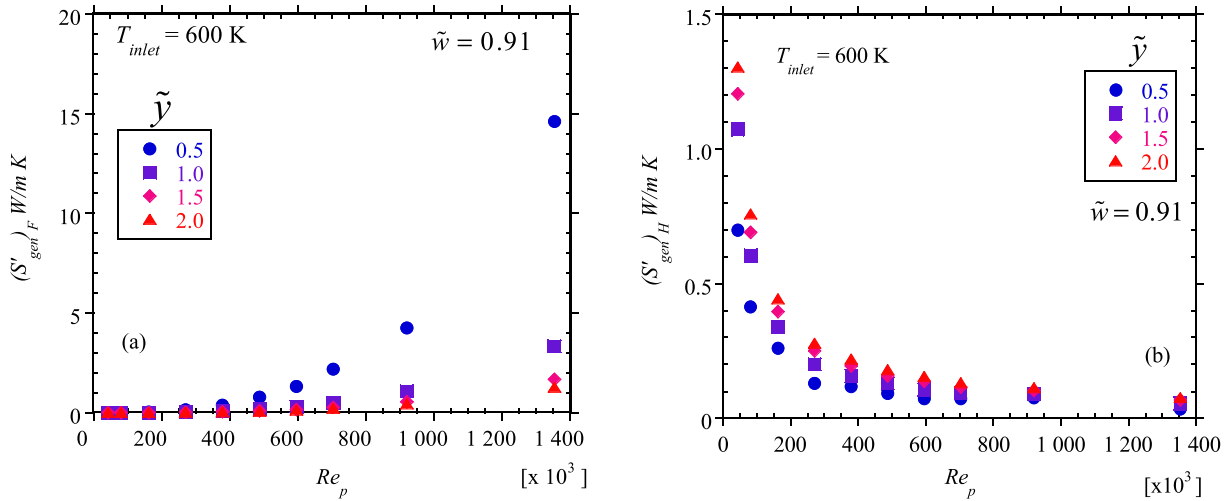

Fig. 22. Entropy generation in the receiver for $T_{inlet} = 600$ K and $\tilde{w} = 0.91$: (a) entropy generation due to fluid flow irreversibilities as a function of Reynolds number and twist ratio and (b) entropy generation due to heat transfer irreversibilities as a function of Reynolds number and twist ratio.
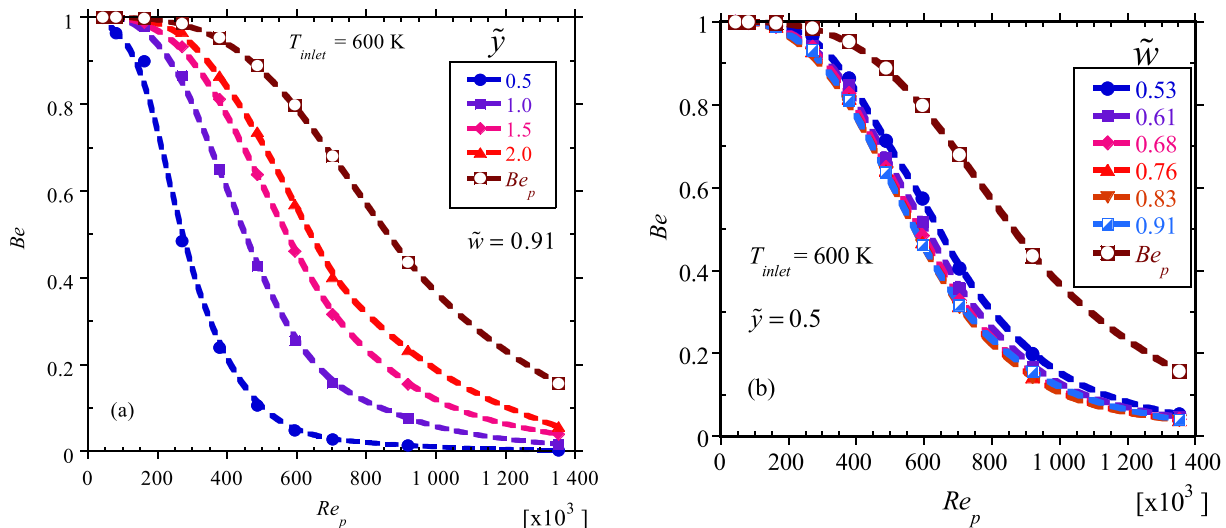

Fig. 23. Bejan number as a function of Reynolds number (a) and twist ratio for $T_{inlet} = 600$ K and $\tilde{w} = 0.91$(b) and width ratio for $T_{inlet} = 600$ K and $\tilde{y} = 0.50$.
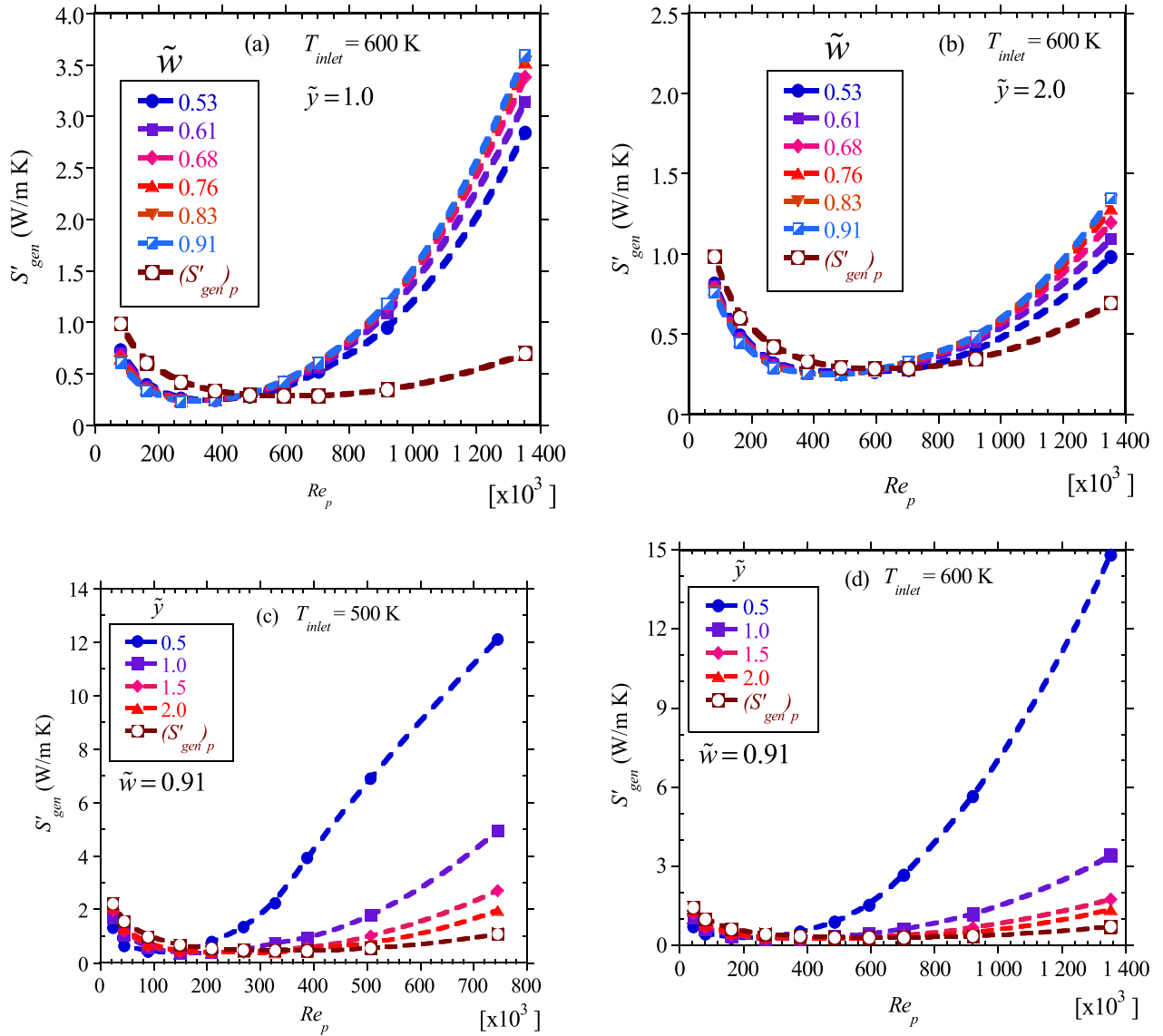
Fig. 24. Total entropy generation rate in the receiver (a) as a function of Reynolds number and width ratio for $T_{inlet} = 600$ K and $\tilde{y} = 1.0$, (b) as a function of Reynolds number and width ratio for $T_{inlet} = 600$ K and $\tilde{y} = 2.0$, (c) as a function of Reynolds number and twist ratio for $T_{inlet} = 500$ K and $\tilde{w} = 0.91$ and (d) as a function of Reynolds number and twist ratio for $T_{inlet} = 600$ K and $\tilde{w} = 0.91$.
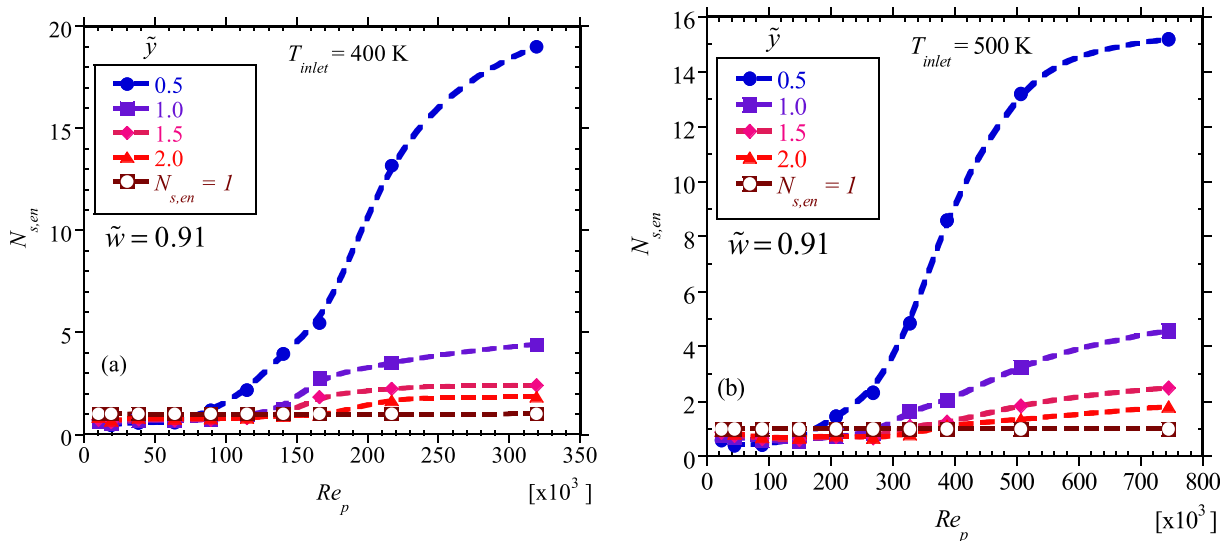

Fig. 25. Entropy generation ratio as a function of Reynolds number and twist ratio for (a) $T_{inlet} = 400$ K and $\tilde{w} = 0.91$ and (b) $T_{inlet} = 500$ K and $\tilde{w} = 0.91$.

with moderate fluid friction increase. From the study, the following observations have been made.

- Due to improved mixing and a longer helical path followed by the heat transfer fluid, high heat transfer enhancement was achieved with the use of wall detached twisted tape inserts.
- Both the heat transfer performance and fluid friction performance increase as the twist ratio reduces and as the width ratio increases. Heat transfer in enhanced in the range 1.05–2.69 times while fluid friction increases in the range 1.6–14.5 compared to a receiver with a plain absorber tube. The thermal enhancement factors for constant pumping power comparison are in the range 0.74–1.27.
- The increase heat transfer performance due to use of twisted tape inserts reduces absorber tube's circumferential temperature difference in the range 4–68%.
- Evaluation of the thermal efficiency using the equation that takes into account the increase in pumping power with heat transfer enhancement shows that the thermal efficiency increases by about 5–10% for flow rates lower than 43 $m^3 h^{-1}$ and twist ratios greater than 1.0.
- Considerable reduction in the entropy generation rates were obtained with the use of twisted tape inserts at low Reynolds numbers. The entropy generation analysis also shows the presence of the optimal Reynolds number at which there is minimum entropy generation for each twist ratio and width ratio. Compared to a plain absorber tube, use of twisted tape inserts reduces the optimal Reynolds number. The optimal Reynolds number was generally observed to increase with an increase in twist ratio and reduction in twist ratio. The maximum reduction in the entropy generation rate was about 58.8%.

Acknowledgment

References

[1] H. Price, E. Lüpfert, D. Kearney, E. Zarza, G. Cohen, R. Gee, R. Mahoney, Advances in parabolic trough solar power technology, Sol. Energy Eng. 124 (2002) 109–125.

[2] H. Price, D. Kearney, Parabolic-Trough Technology Roadmap: a Pathway for Sustained Commercial Development and Deployment of Parabolic Trough Technology, NREL Technical Report, NREL/TP-550-24748, January 1999, pp. 1–35.

[3] H. Price, D. Kearney, Reducing the Cost of Energy from Parabolic Trough Solar Power Plants, NREL Technical Report, NREL/CP-550-33208, 2003, pp. 1–9.

[4] SunShot Initiative, U. S Department of Energy. Available at: http://www1.eere.energy.gov/solar/sunshot/index.html (last accessed 12.11.14).

[5] SunShot Initiative. High-Concentration Low Cost Parabolic Trough System for Baseload CSP, U.S. Department of Energy. Available at: http://www1.eere.energy.gov/solar/sunshot/csp_baseload_skyfuel.html (last accessed 12.11.14).

[6] Skyfuel, SkyTrough® Product Information: Next-Generation Solar Parabolic Tough Technology, 2011. http://www.skyfuel.com/downloads/brochure/skytroughbrochure.pdf (last accessed 21.04.15).

[7] A.E. Bergles, Techniques to enhance heat transfer, in: J.P. Hartnett, Y.I. Cho (Eds.), Handbook of Heat Transfer, McGraw-Hill, New York, 1998, pp. 11.71–11.76.

[8] R.M. Manglik, Heat transfer enhancement, in: A. Bejan, A.D. Kraus (Eds.), Heat Transfer Handbook, John Wiley & Sons, Hoboken, New Jersey, 2003, pp. 1029–1130.

[9] R.L. Webb, Principles of Enhanced Heat Transfer, John Wiley & Sons, New York, 1994.

[10] J. Muñoz, A. Abánades, Analysis of internal helically finned tubes for parabolic trough design by CFD tools, Appl. Energy 88 (2011) 4139–4149.

[11] E. Lüpfert, M. Pfänder, B. Schiricke, M. Eck, Determination of temperature distribution on parabolic trough receivers, in: 13th International Symposium on Concentrating Solar Power and Chemical Energy Technologies, Solar-PACES2006, 2006. A1-S6.

[12] F. Burkholder, C. Kutscher, Heat-Loss Testing of Solel's UVAC3 Parabolic Trough Receiver, NREL Technical Report, NREL/TP-550-42394, 2008, pp. 1–19.

[13] E. Lüpfert, K. Riffelmann, H. Price, F. Burkholder, T. Moss, Experimental analysis of overall thermal properties of parabolic trough receivers, Sol. Energy Eng. 130 (2008) 021007.

[14] K. Ravi Kumar, K.S. Reddy, Numerical investigation of energy-efficient receiver for solar parabolic trough concentrator, Heat Transf. Eng. 29 (2008) 961–972.

[15] K. Ravi Kumar, K.S. Reddy, Thermal analysis of solar parabolic trough with porous disc receiver, Appl. Energy 86 (2009) 1804–1812.

[16] Z.D. Cheng, Y.L. He, F.Q. Cui, Numerical study of heat transfer enhancement by unilateral longitudinal vortex generators inside parabolic trough solar receivers, Int. J. Heat Mass Transf. 55 (2012) 5631–5641.

[17] A.E. Bergles, ExHFT for fourth generation heat transfer technology, Exp. Therm. Fluid Sci. 26 (2002) 335–344.

[18] R.M. Manglik, A.E. Bergles, Swirl flow heat transfer and pressure drop with twisted-tape inserts, in: J.P. Hartnett, T.F. Irvine, Y.I. Cho, G.A. Greene (Eds.), Advances in Heat Transfer, Academic Press, San Diego, California, 2002, pp. 183–266.

[19] A. Hasanpour, M. Farhadi, K. Sedighi, A review study on twisted tape inserts on turbulent flow heat exchangers: the overall enhancement ratio criteria, Int. Commun. Heat Mass Transf. 55 (2014) 53–62.

[20] S. Liu, M. Sakr, A comprehensive review on passive heat transfer enhancements in pipe exchangers, Renew. Sustain. Energy Rev. 19 (2013) 64–81.

[21] C.K. Nithiyesh, P. Murugesan, Review on twisted tapes heat transfer enhancement, IJSER 3 (2012) 1–9.

[22] S. Jaisankar, T.K. Radhakrishnan, K.N. Sheeba, Experimental studies on heat transfer and friction factor characteristics of forced circulation solar water heater system fitted with helical twisted tapes, Sol. Energy 83 (2009) 1943–1952.

[23] S. Jaisankar, T.K. Radhakrishnan, K.N. Sheeba, Studies on heat transfer and friction factor characteristics of thermosyphon solar water heating system with helical twisted tapes, Energy 34 (2009) 1054–1064.

[24] S. Jaisankar, T.K. Radhakrishnan, K.N. Sheeba, Experimental studies on heat transfer and thermal performance characteristics of thermosyphon solar water heating system with helical and left–right twisted tapes, Energy Convers. Manag. 52 (2011) 2048–2055.

[25] S. Jaisankar, T.K. Radhakrishnan, K.N. Sheeba, S. Suresh, Experimental investigation of heat transfer and friction factor characteristics of thermosyphon solar water heater system fitted with spacer at the trailing edge of left–right twisted tapes, Energy Convers. Manag. 50 (2009) 2638–2649.

[26] E. Esmaeilzadeh, H. Almohammadi, A. Nokhosteen, A. Motezaker, A.N. Omrani, Study on heat transfer and friction factor characteristics of γ-Al₂O₃/water through circular tube with twisted tape inserts with different thicknesses, Int. J. Therm. Sci. 82 (2014) 72–83.

[27] W.H. Azmi, K.V. Sharma, P.K. Sarma, R. Mamat, S. Anuar, Comparison of convective heat transfer coefficient and friction factor of TiO₂ nanofluid flow in a tube with twisted tape inserts, Int. J. Therm. Sci. 81 (2014) 84–93.

[28] L. Moens, D.M. Blake, Mechanism of hydrogen formation in solar parabolic trough receivers, J. Sol. Energy-Trans. ASME 132 (2010) 031006.

[29] Z.H. Ayub, S.F. Al-Fahed, The effect of gap width between horizontal tube and twisted tape on the pressure drop in turbulent water flow, Int. J. Heat Fluid Flow 14 (1993) 64–67.

[30] S. Al-Fahed, W. Chakroun, Effect of tube-tape clearance on heat transfer for fully developed turbulent flow in a horizontal isothermal tube, Int. J. Heat Fluid Flow 17 (1996) 173–178.

[31] S. Eiamsa-ard, K. Wongcharee, S. Sripattanapipat, 3-D numerical simulation of swirling flow and convective heat transfer in a circular tube induced by means of loose-fit twisted tapes, Int. Commun. Heat Mass Transf. 36 (2009) 947–955.

[32] X. Zhang, Z. Liu, W. Liu, Numerical studies on heat transfer and flow characteristics for laminar flow in a tube with multiple regularly spaced twisted tapes, Int. J. Therm. Sci. 58 (2012) 157–167.

[33] H. Bas, V. Ozceyhan, Heat transfer enhancement in a tube with twisted tape inserts placed separately from the tube wall, Exp. Therm. Fluid Sci. 41 (2012) 51–58.

[34] A. Bejan, Entropy Generation Minimization: the Method of Thermodynamic Optimization of Finite-Size Systems and Finite-Time Processes, CRC Press, Boca Raton, Fla., 1996.

[35] A. Bejan, A study of entropy generation in fundamental convective heat transfer, J. Heat Transf. 101 (1979) 718–725.

[36] E.V. Dudley, J.G. Kolb, A.R. Mahoney, T. Mancini, R.,M. Sloan, D. Kearney, Test Results: SEGS LS-2 Solar Collector, SAND94-1884, Sandia National Laboratory, 1994.

[37] ANSYS® Academic research, release 14.5, ANSYS FLUENT, Theory Guide, ANSYS, Inc.

[38] H.K. Versteeg, W. Malalasekera, An Introduction to Computational Fluid Dynamics: the Finite Volume Method, second ed., Pearson/Prentice Hall, Harlow, England, 2007.

[39] T. Shih, W.W. Liou, A. Shabbir, Z. Yang, J. Zhu, A new k−ε eddy viscosity model for high Reynolds number turbulent flows, Comput. Fluids 24 (1995) 227–238.

[40] F. Kock, H. Herwig, Entropy production calculation for turbulent shear flows and their implementation in CFD codes, Int. J. Heat Fluid Flow 26 (2005) 672–680.

[41] W.G. Le Roux, T. Bello-Ochende, J.P. Meyer, Optimum performance of the small-scale open and direct solar thermal Brayton cycle at various environmental conditions and constraints, Energy 46 (2012) 42–50.

[42] T.H. Ko, A numerical study on developing laminar forced convection and entropy generation in half- and double-sine ducts, Int. J. Therm. Sci. 46 (2007) 1275–1284.

[43] A.K. Satapathy, Thermodynamic optimization of a coiled tube heat exchanger under constant wall heat flux condition, Energy 34 (2009) 1122–1126.

[44] A. Mwesigye, T. Bello-Ochende, J.P. Meyer, Numerical investigation of entropy generation in a parabolic trough receiver at different concentration ratios, Energy 53 (2013) 114–127.

[45] A. Bejan, The thermodynamic design of heat and mass transfer processes and devices, Int. J. Heat Fluid Flow 8 (1987) 258–276.

[46] V.D. Zimparov, N.L. Vulchanov, Performance evaluation criteria for enhanced heat transfer surfaces, Int. J. Heat Mass Transf. 37 (1994) 1807–1816.

[47] V.D. Zimparov, P.J. Penchev, Performance evaluation of some tube inserts as heat transfer enhancement techniques, Heat Transf. Eng. 27 (2006) 39–46.

[48] W.R. Oullette, A. Bejan, Conservation of available work (exergy) by using promoters of swirl flow in forced convection heat transfer, Energy 5 (1980) 587–596.

[49] SolTrace Optical Modelling Software, SolTrace v2012.7.9.

[50] W.C. Swinbank, Long-wave radiation from clear skies, Q. J. R. Meteorol. Soc. 89 (1963) 339–348.

[51] S.C. Mullick, S.K. Nanda, An improved technique for computing the heat loss factor of a tubular absorber, Sol. Energy 42 (1989) 1–7.

[52] S.V. Patankar, D.B. Spalding, A calculation procedure for heat, mass and momentum transfer in three-dimensional parabolic flows, Int. J. Heat Mass Transf. 15 (1972) 1787–1806.

[53] Dow, Syltherm800 heat transfer fluid: product technical data. http://www.dow.com/heattrans/products/synthetic/syltherm.htm (last accessed 12.06.14).

[54] R. Forristall, Heat Transfer Analysis and Modeling of a Parabolic Trough Solar Receiver Implemented in Engineering Equation Solver, NREL Technical Report, NREL/TP-550-34169, October 2003, pp. 1–145.

[55] Y.A. Çengel, A.J. Ghajar, Heat and Mass Transfer: Fundamentals & Applications, fourth ed., McGraw-Hill, New York, 2011.

[56] R.M. Manglik, A.E. Bergles, Heat transfer and pressure drop correlation for twisted-tape inserts in isothermal tubes: part II – transition and turbulent flows, J. Heat Transf. 115 (1993) 890–896.

[57] M. Wirz, J. Petit, A. Haselbacher, A. Steinfeld, Potential improvements in the optical and thermal efficiencies of parabolic trough concentrators, Sol. Energy 107 (2014) 398–414.